# EXISTENCE OF THE MANDELBROT SET IN THE PARAMETER PLANES OF CERTAIN RATIONAL FUNCTIONS

by

Alexander Mitchell

A Dissertation Submitted in

Partial Fulfillment of the

Requirements for the Degree of

Doctor of Philosophy

in Mathematics

at

The University of Wisconsin-Milwaukee

August 2016

ABSTRACT

EXISTENCE OF THE MANDELBROT SET
IN THE PARAMETER PLANES
OF CERTAIN RATIONAL FUNCTIONS

by

Alexander Mitchell

The University of Wisconsin-Milwaukee, 2016
Under the Supervision of Professor Suzanne Boyd

In complex dynamics we compose a complex valued function with itself repeatedly and observe the orbits of values of that function. Particular interest is in the orbit of critical points of that function (critical orbits). One famous, studied example is the quadratic polynomial $P_c(z) = z^2 + c$ and how changing the value of $c$ makes a difference to the orbit of the critical point $z = 0$. The set of $c$ values for which the critical orbit is bounded is called the Mandelbrot set.

This paper studies rational functions of the form $R_{n,a,c}(z) = z^n + \frac{a}{z^n} + c$ and their critical orbits. It turns out that for certain fixed values of $n$, $a$, and $c$, $R_{n,a,c}$ locally behaves like $P_c$. On those regions $R_{n,a,c}$ is said to be a *degree two polynomial-like map*.

We then consider fixing $a$ while allowing $c$ to vary and study the $a$-parameter plane of $R_{n,a,c}$ and then vice-versa. We show that homeomorphic copies of the Mandelbrot set exist in both the $a$ and $c$-parameter planes. Finally we observe peculiar behaviors of the parameter planes when multiple Mandelbrot copies exist and are in close proximity to each other.

# TABLE OF CONTENTS

# LIST OF FIGURES

# Chapter 1

# Introduction

## 1.1 Background

Complex dynamics is the study of **iteration**, which is the process of composing a single function $f$ with itself repeatedly. The background of complex dynamics given in this section can be studied further in a textbook such as [GC93] or [Bea91].

A simple starting example is the squaring function, $P_0(z) = z^2$. As we compose this function with itself, we get the sequence of iterates $\{P_0^k(z) = z^{2^k}\}$. If we pick a value $z_0$ in the domain of $f$, then the **orbit** of $z_0$ under $f$ is the set of all iterates of $f$ evaluated at $z_0$; that is the sequence

$$\{z_0, z_1 = f(z_0), \ldots, z_n = f(z_{n-1}) = f^n(z_0), \ldots\}.$$

Typically we are interested in what happens as the number of iterates become very large. Does the orbit tend to a single point or a cycle of points? Does the orbit stay bounded or become unbounded? Perhaps it does not tend to anything and there is no easily describable limiting behavior.

The domain of $f$ can be partitioned into two sets based on orbits in the domain. A value $z$ is in the **Fatou set** of $f$ if the sequence of iterates of $f$ is normal in some neighborhood of

$z$ (i.e., the sequence has a subsequence that converges uniformly on every compact subset of that neighborhood of $z$). These can be thought of as the points whose orbits under $f$ behave "nicely". The complement to this set is called the **Julia set** of $f$. These are the points that do not have an easily described limiting behavior to their orbit. For polynomials, the **filled Julia set** of $f$ is the union of the Julia set and bounded Fatou components of $f$. For polynomials $\infty$ is a super-attracting fixed point, and the rational functions we study also have that characteristic.

(a) $c = 0$ (b) $c = -1$ (c) $c = -0.131 + 0.769i$

Figure 1.1: A few filled Julia sets (pictured in black) of $P_c$ for different values of $c$

As a starting example, we consider what the Julia and Fatou sets of $P_0$ are. Letting $k$ grow large for $P_0^k$ as $k$, the orbit of any value $z$ such that $|z| < 1$ will tend to 0 and any $z$ value such that $|z| > 1$ will tend to $\infty$. Therefore those values are all in the Fatou set of $P_0$. The complement to this is the unit circle and is thus the Julia set of $P_0$. The closed unit disk is the filled Julia set of $P_0$, pictured in Figure 1.1a.

The Fatou and Julia sets of most functions are not so simple to describe. A quick example is adding a constant to $P_0$, like $P_{-1}(z) = z^2 - 1$. We lose the ability to write an explicit expression for $P_{-1}^k$ and find the Julia set to have an intricate structure. Figure 1.1b gives a picture of the "Basilica" Julia set of $P_{-1}$. Another example is the "Douady's Rabbit" Julia set given in Figure 1.1c. In these pictures the black is the filled Julia set and the boundary is the Julia set itself. Figures provided throughout this paper were generated using the program DeTool [BB].

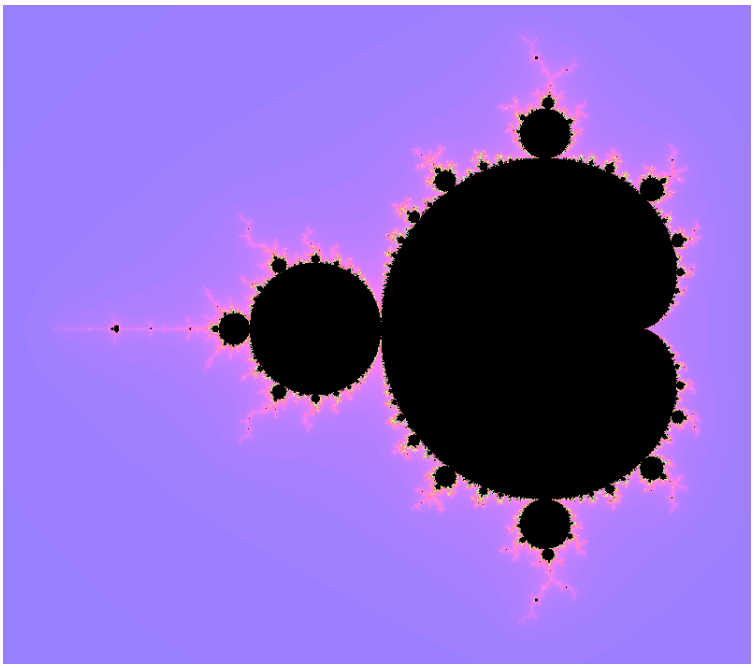

Figure 1.2: The Mandelbrot Set of $P_c$

There are particular components of the Fatou set of $f$ that are of interest to us. For instance if several orbits approach the same value $z_0$ under $f$, then those set of values are in the **basin of attraction** of $z_0$ (denoted $A(z_0)$). The connected component of $A(z_0)$ that contains $z_0$ is called the **immediate basin of attraction** of $z_0$ (denoted $A^*(z_0)$) and will be of interest to us later. $A^*(\infty)$ is the orange region in each of the pictures of Figure 1.1. The shading of each point of $A^*(\infty)$ is determined by how fast the orbit of that point escapes to $\infty$. The quicker an orbit escapes, the darker the shade of orange will be assigned to that value by the program.

The behavior of an individual function is observed in the **dynamical plane** of that function. We can add a constant to $z^2$ to generate $P_c(z) = z^2 + c$, and we now have a family of functions indexed by $c$. We ask how the dynamics of $P_c$ changes with $c$. All of this will be observed in the $c$-**parameter plane** of $P_c$.

We cannot look into the orbit of every single value for this general case so we focus on the orbit of critical points (denoted **critical orbit**) instead. The critical point of $P_c$ is 0 and we ask how the critical orbit changes with $c$.

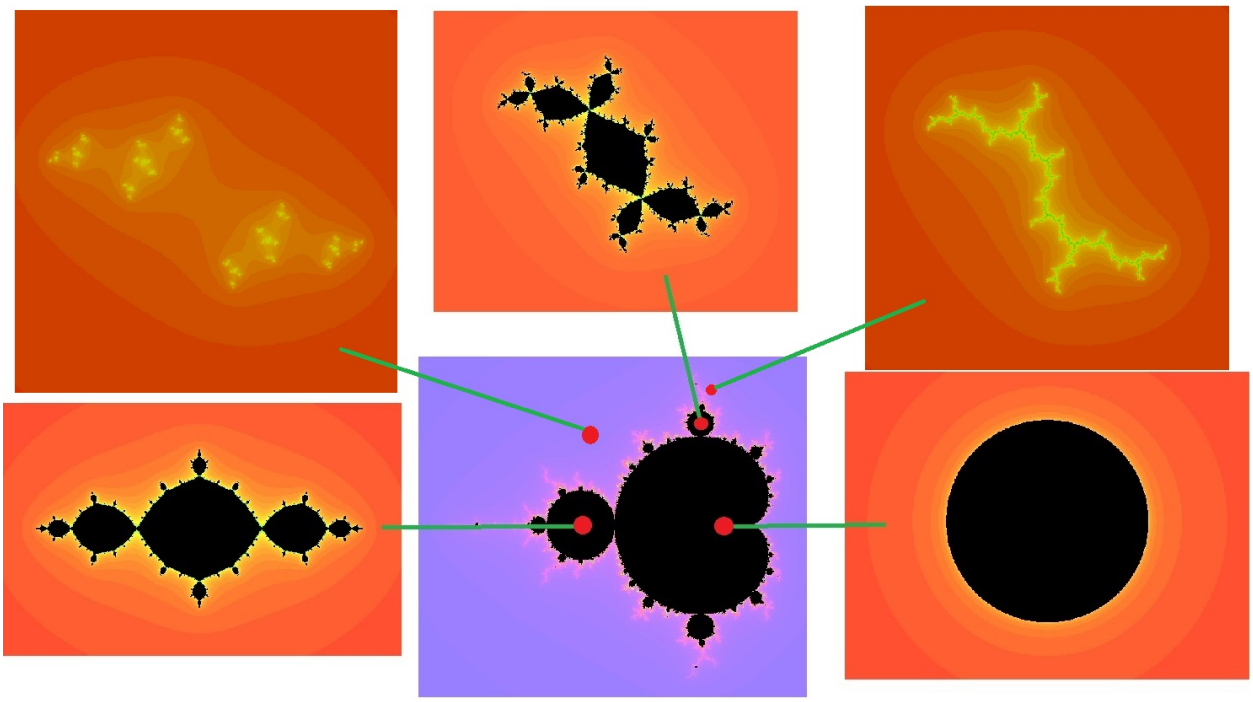

Figure 1.3: Various Julia sets spawned from the Mandelbrot Set

The set of values in the $c$-parameter plane for which the critical orbit of $P_c$ is bounded is called the **Mandelbrot set**, pictured in Figure 1.2. This set will be hereafter denoted by $\mathcal{M}$. $\mathcal{M}$ has been studied extensively since the advent of super computers in the 1980's and the fractal nature of $\mathcal{M}$ is still an active topic of research. The connected components of $\mathcal{M}$ categorize the critical orbit of $P_c$ for different values of $c$. For instance, the central cardioid structure of $\mathcal{M}$ is where $c = 0$ lies and the critical orbit of $P_c$ tends to a fixed point for any $c$ in the main cardioid. In fact, the filled Julia set of $P_c$ is a topological disk for any $c$-value in that main cardioid and $c$-values lying in other connected components of $\mathcal{M}$ yield a similar behavior.

Another known result from polynomial complex dynamics is if all critical orbits of a function are bounded then the Julia set of that function is connected. Therefore all functions 'spawned' from $\mathcal{M}$ have a connected Julia set. Figure 1.3 shows examples of different Julia sets spawned from parameter values chosen inside and out of $\mathcal{M}$.

## 1.2 The Dynamics of $R_{n,a,0}$

We study these concepts for the family of functions $R_{n,a,0} = z^n + \frac{a}{z^n}$ with $n \geq 3$, and $a \in \mathbb{C}\backslash\{0\}$. We observe that now 0 is a pole of this function and $\infty$ is a superattracting fixed point. This being a similar behavior to polynomials, we define the **filled Julia set** of $R_{n,a,0}$ to be the complement of all pre-images of $A^*(\infty)$, or the points whose orbits avoid $\infty$. The first pre-image of $\infty$ is 0 and we will define $T_a$ as the pre-image of $A^*(\infty)$ that contains 0. This set has been called the **trap door** because the orbit of any pre-image of $A^*(\infty)$ (excluding $A^*(\infty)$ itself) must pass through $T_a$.

$R_{n,a,0}$ has $2n$ critical points, $a^{\frac{1}{2n}}$, which makes for a large number of critical orbits to observe as $n$ increases. Note though that the images of the critical points (the **critical values**) are

$$v_{\pm} = R_{n,a,0}(a^{\frac{1}{2n}}) = \pm 2\sqrt{a}.$$

Thus the $2n$ critical points map into two critical orbits. Even further, all critical orbits of $R_{n,a,0}$ are symmetric [Dev06] and this means there is only one **free critical orbit** to keep track of. This makes it simple to draw the $a$-parameter plane of $R_{n,a,c}$ for a given $n$. We color each $a$-value based on whether the critical orbit is bounded or not. Figure 1.4 gives one example of the $a$-parameter plane of $R_{5,a,0}$.

We call the set of $a$-values for which the critical orbit does not escape to $\infty$ the **boundedness locus**. It is shown in [Dev06] that the boundedness locus is contained in $|a| \leq 1$. A point is colored black if the critical orbit for that $a$-value is bounded and blue otherwise. A striking phenomenon is there seem to be copies of $\mathcal{M}$ lying in this parameter plane (as seen in Figure 1.4). These figures are in fact homeomorphic copies of $\mathcal{M}$ and each will henceforth be referred to as a **baby** $\mathcal{M}$ [Dev06]. Robert Devaney proved that for $n \geq 3$, there are $n-1$ baby $\mathcal{M}$'s lying in the $a$-plane of $R_{n,a,0}$ and they are rotationally symmetric about the origin.

Results in the dynamical planes of $R_{n,a,0}$ are where to start in order to prove results in the parameter plane. Devaney has shown for $|a| \leq 1$ and $|z| \geq 2$ that $z \in A^*(\infty)$. This

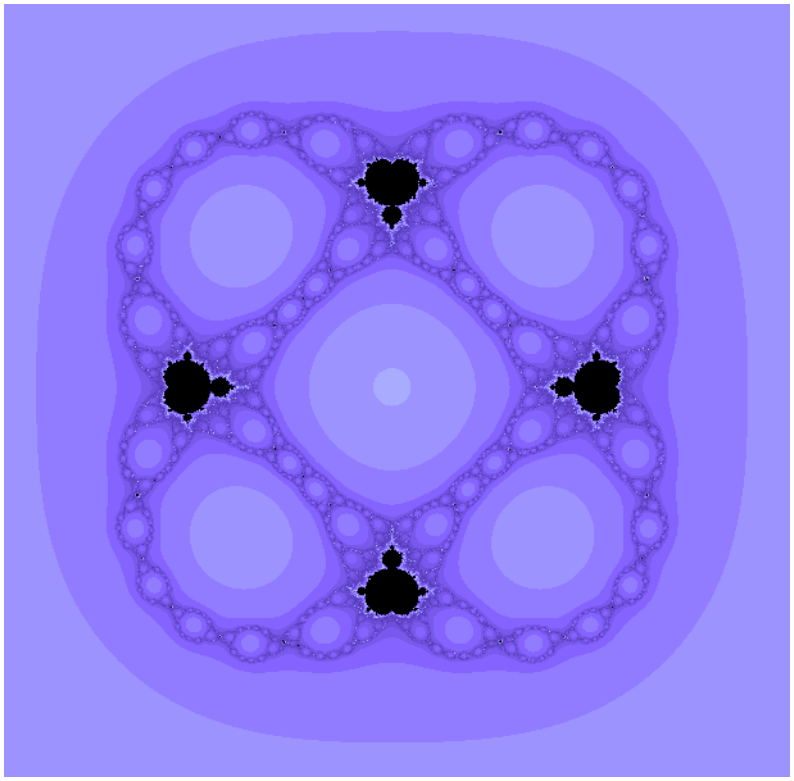

Figure 1.4: $a$-parameter plane of $R_{n,a,c}$ for $n = 5$ and $c = 0$

means the filled Julia set of $R_{n,a,0}$ lies within the disk of radius 2 centered at the origin ($\mathbf{D}(0, 2)$). In [Dev06] it is also shown there are symmetries of $R_{n,a,0}$ and the filled Julia set is restricted further to lying in the annulus between the radii of $\frac{|a|^{\frac{1}{n}}}{2}$ and 2. This gives an **Escape Criterion** for the orbits of $R_{n,a,0}$.

Devaney and collaborators also prove a result about the topology of the Julia set of $R_{n,a,0}$ given that $a$ is chosen such that the critical orbit escapes to $\infty$ [RLD05].

**Theorem 1.1.** *(The Escape Trichotomy). Suppose that the free critical orbit of $R_{n,a,0}$ tends to $\infty$. Then*

1. *If $v_{\pm}$ lie in $A^*(\infty)$, then the Julia set of $R_{n,a,0}$ is a Cantor set;*

2. *If $v_{\pm}$ lie in $T_a$, then the Julia set of $R_{n,a,0}$ is a Cantor set of simple closed curves;*

3. *If $v_{\pm}$ do not lie in either $A^*(\infty)$ or $T_a$, then the Julia set of $R_{n,a,0}$ is a connected set. Further if $v_{\pm}$ lie in some other pre-image of $A^*(\infty)$, then the Julia set is a Sierpinski*

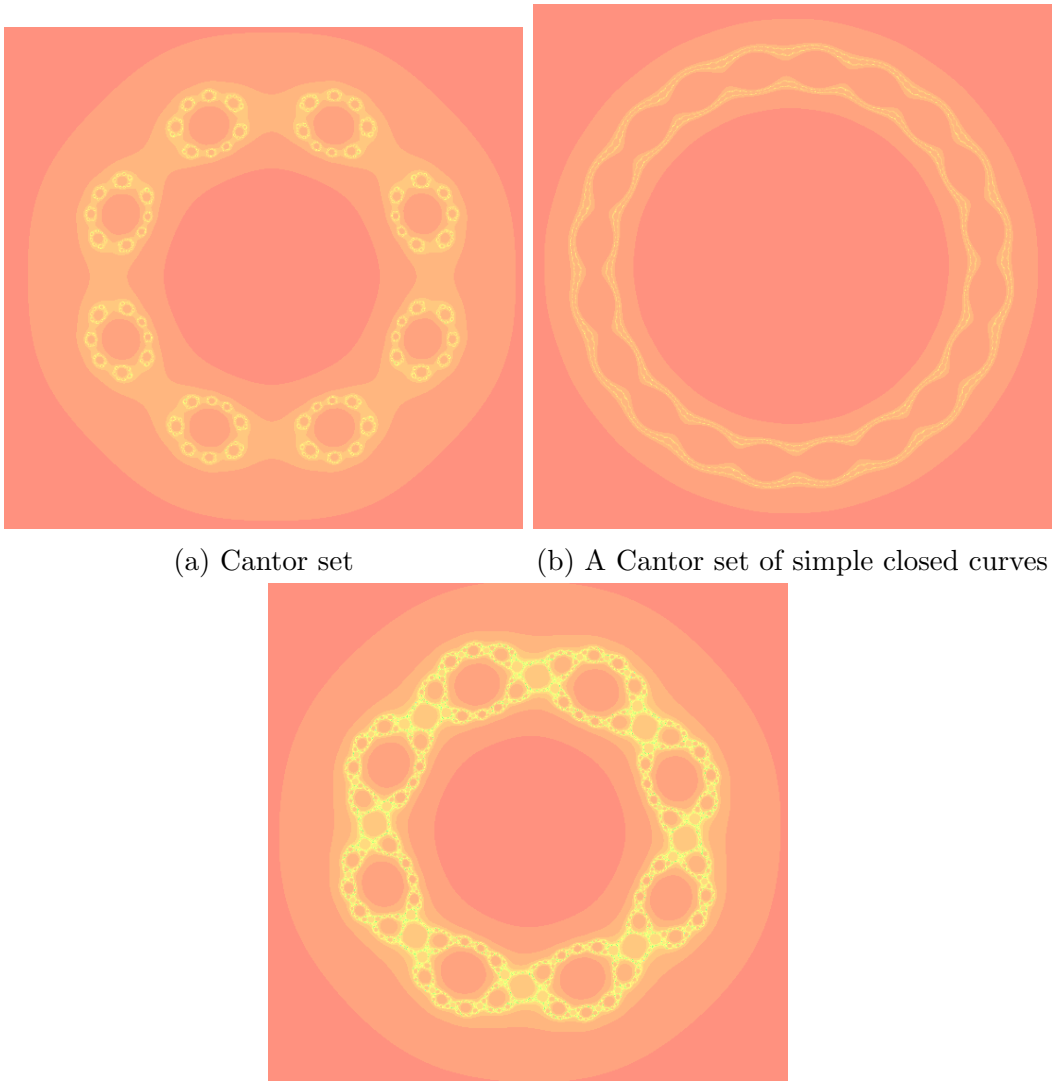

(a) Cantor set

(b) A Cantor set of simple closed curves

(c) A Sierpinski curve

Figure 1.5: Example Julia sets of $R_{n,a,0}$ associated with the escape trichotomy.

*Curve.*

## 1.3 Polynomial-Like Maps

To prove the existence of baby $\mathcal{M}$'s in the parameter plane, Devaney used tools and techniques developed by Douady and Hubbard in [DH85]. These tools consist of showing how the dynamics of $R_{n,a,0}$ behave locally like a degree two polynomial.

**Definition 1.2.** *([DH85]) Suppose* $\mathbf{U}'$ *and* $\mathbf{U}$ *are bounded, open, simply connected subsets of* $\mathbb{C}$ *and* $\mathbf{U}' \subset \mathbf{U}$ *with* $\mathbf{U}'$ *relatively compact in* $\mathbf{U}$*. A map* $F : \mathbf{U}' \to \mathbf{U}$ *is* ***polynomial-like*** *if* $F$ *is analytic and proper.*

The map is polynomial-like of degree two if it is a 2-to-1 map with a unique critical point in $\mathbf{U}'$. The filled Julia set of a polynomial-like map is the set of values whose orbits do not escape $\mathbf{U}'$. Douady and Hubbard showed why this name is a natural one.

**Theorem 1.3.** *[DH85] A polynomial-like map of degree two is topologically conjugate on its filled Julia set to a quadratic polynomial on that polynomial's filled Julia set.*

This establishes that such a map locally has the same dynamics as a quadratic polynomial. Figures given later will help to establish visual evidence of this connection. Douady and Hubbard also proved an important result about families of degree two polynomial-like maps.

**Theorem 1.4.** *[DH85] Assume we are given a family of polynomial-like maps* $F_\lambda : \mathbf{U}'_\lambda \to \mathbf{U}_\lambda$ *that satisfies the following:*

1. $\lambda$ *is in an open set in* $\mathbb{C}$ *which contains a closed disk* $W$*;*
2. *The boundaries of* $\mathbf{U}'_\lambda$ *and* $\mathbf{U}_\lambda$ *vary analytically as* $\lambda$ *varies;*
3. *The map* $(\lambda, z) \mapsto F_\lambda(z)$ *depends analytically on both* $\lambda$ *and* $z$*;*
4. *Each* $F_\lambda$ *is polynomial-like of degree two with a unique critical point* $c_\lambda$ *in* $\mathbf{U}'$*.*

*Suppose that for all* $\lambda \in \partial W$ *that* $F_\lambda(c_\lambda) \in \mathbf{U} - \mathbf{U}'$*. and that* $F_\lambda(c_\lambda)$ *makes a closed loop around the outside of* $\mathbf{U}'$ *as* $\lambda$ *winds once around* $\partial W$*. If all this occurs, then the set of* $\lambda$*-values for which the orbit of* $c_\lambda$ *does not escape from* $\mathbf{U}'$ *is homeomorphic to the Mandelbrot set.*

This is the process of which we will recreate in order to prove the existence of baby $\mathcal{M}$'s. Devaney used this technique to prove the existence of a single baby $\mathcal{M}$ in the $a$-parameter

plane of $R_{n,a,0}$ for all $n \geq 3$. Further he showed there was a rotational symmetry among the critical orbits and this yielded the existence of $n-1$ 'principal' baby $\mathcal{M}$'s in the $a$-parameter plane. He calls these principal because there are more that exist in the parameter plane but they are increasingly smaller. In [Dev09a], Devaney shows there are actually infinitely many disjoint baby $\mathcal{M}$'s in the parameter plan of $R_{n,a,0}$ for $n \geq 3$. The homeomorphic copies of the Mandelbrot set found in this paper shall be referred to as baby $\mathcal{M}$'s.

## 1.4 Main Results

The family of functions we study is $R_{n,a,c} = z^n + \dfrac{a}{z^n} + c$ for $c \neq 0$. This case takes a leap in complexity compared to the $c = 0$ case. With more parameters to control, careful observation must be taken. Also the symmetries within this family are not as evident. In this paper we find the critical orbits of this family still have the same dynamics as the critical orbit of $P_c$ locally, and thus there are copies of the Mandelbrot set in both the $a$ and $c$ parameter planes of $R_{n,a,c}$. Specifically:

**Theorem 3.3.** *For $n \geq 3$, $-1 \leq c \leq 0$ there exists in the $a$-parameter plane a homeomorphic copy of the Mandelbrot set associated with one of the critical orbits of $R_{n,a,c}$.*

and also:

**Theorem 3.12.** *For odd $n \geq 3$, and $1 \leq a \leq \dfrac{(2^{n+1}-8)^2}{16}$ there exist $2n$ homeomorphic copies of the Mandelbrot set in the $c$-parameter plane of $R_{n,a,c}$, half of which are associated with one critical orbit, and the other half associated with the opposite critical orbit. (See Figure 1.6 for an example.)*

Within chapter 2 we will establish results about some symmetries of $R_{n,a,c}$ as well as the location of the Julia set of $R_{n,a,c}$. We also establish the fact that locally $R_{n,a,c}$ is a polynomial-like map of degree two. Using these results we can show that the dynamical planes of $R_{n,a,c}$ contain homeomorphic copies of quadratic Julia sets of $P_c$.

In Chapter 3 we will investigate the parameter planes of $R_{n,a,c}$ and show the existence of

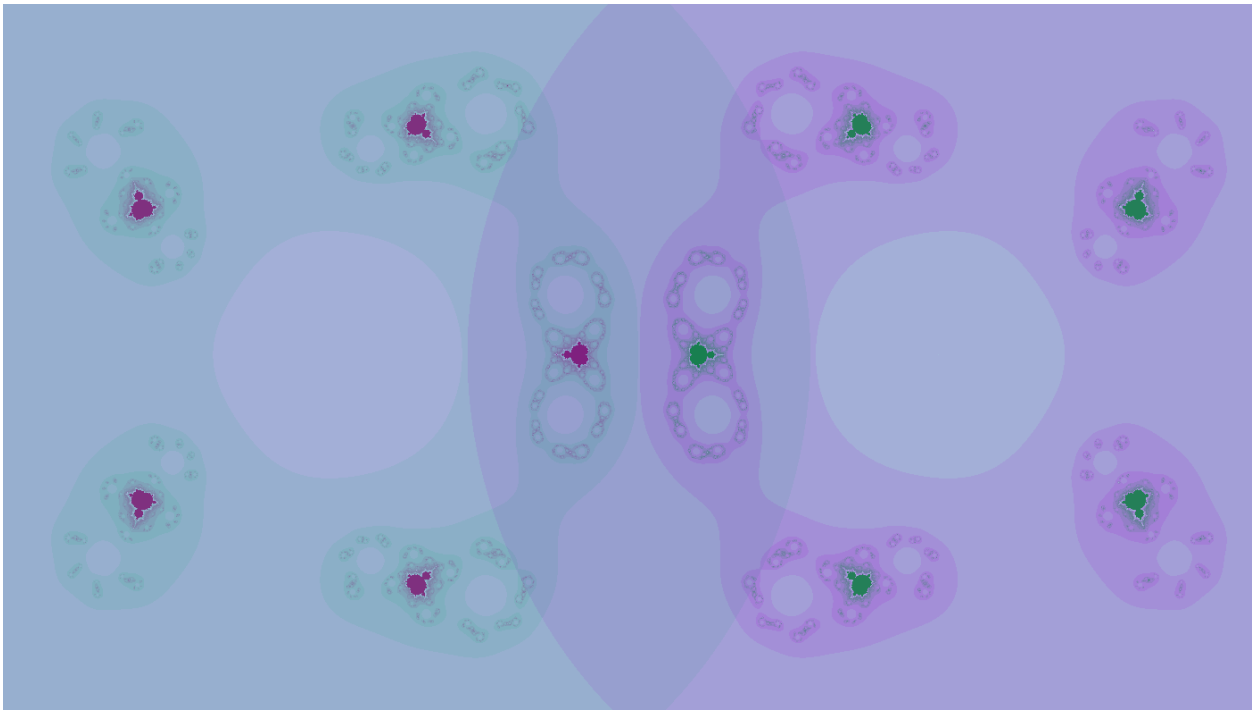

Figure 1.6: The $c$-parameter plane of $R_{n,a,c}$ with $n = 5$ and $a = 0.3$.

baby $\mathcal{M}$ lying in these parameter planes using the tools discussed in the introduction.

Lastly chapter 4 starts a brief discussion into further possibilities of study with a glimpse at some interesting behavior occurring in the parameter planes. Certain situations in the $a$ and $c$-parameter planes seem to create the existence of small copies of Julia sets of individual quadratic maps.

# Chapter 2

# The Family of Functions

$$R_{n,a,c} = z^n + \frac{a}{z^n} + c$$

We define the family of degree $2n$ rational functions

$$R_{n,a,c} = z^n + \frac{a}{z^n} + c$$

where $n \geq 3$, $a \in \mathbb{C}\backslash\{0\}$, and $c \in \mathbb{C}$. Here we define the **filled Julia set** of $R_{n,a,c}$ the same as the $c = 0$ case from the introduction. In this chapter we will establish properties of this family that follow in parallel to the $c = 0$ case. We will show there are a number of symmetries that exist and take advantage of them as well as create criterion for the location of the Julia set of $R_{n,a,c}$.

$R_{n,a,c}$ has $2n$ critical points, $a^{\frac{1}{2n}}$, but

$$v_{\pm} = R_{n,a,c}(a^{\frac{1}{2n}}) = c \pm 2\sqrt{a}$$

and there are really only two free critical orbits to track.

## 2.1 Symmetries of $R_{n,a,c}$

The following discusses a number of symmetries of the family $R_{n,a,c}$. We will take advantage of these results all throughout this paper and thus often refer back to this section. The first is an involution symmetry.

**Proposition 2.1.** *$R_{n,c,a}$ is symmetric under the involution map $h_a(z) = \frac{a^{\frac{1}{n}}}{z}$.*

*Proof.*

$$R_{n,c,a}(h_a(z)) = \left(\frac{a^{\frac{1}{n}}}{z}\right)^n + \frac{a}{\left(\frac{a^{\frac{1}{n}}}{z}\right)^n} + c = \frac{a}{z^n} + z^n + c = R_{n,c,a}(z).$$

□

This symmetry shows that neighborhoods of the origin will map to neighborhoods of $\infty$. When determining the structure and position of the Julia set of $R_{n,a,c}$, Proposition 2.1 will help. The next few symmetries focus on negatives and complex conjugates.

**Lemma 2.2.** *For $n$ odd, $R^k_{n,a,-c}(-z) = -R^k_{n,a,c}(z)$ where $k$ is the $k^{th}$ iterate of $R$*

*Proof.* We prove this inductively, so let the base case be the first iterate of $R_{n,a,c}$:

$$\begin{aligned} R_{n,a,-c}(-z) &= (-z)^n + \frac{a}{(-z)^n} - c \\ &= -z^n - \frac{a}{z^n} - c \ (Since\ n\ is\ odd) \\ &= -\left(z^n + \frac{a}{z^n} + c\right) \\ &= -R_{n,a,c}(z). \end{aligned}$$

Now assuming the hypothesis is true for $k-1$, $R^{k-1}_{n,a,-c}(-z) = -R^{k-1}_{n,a,c}(z)$, then

$$\begin{aligned} R^k_{n,a,-c}(-z) &= R^{k-1}_{n,a,-c}(R_{n,a,-c}(-z)) \\ &= R^{k-1}_{n,a,-c}(-(R_{n,a,c}(z))) \ (from\ the\ base\ case) \\ &= -R^{k-1}_{n,a,c}(R_{n,a,c}(z)) \ (from\ the\ inductive\ assumption) \\ &= -R^k_{n,a,c}(z). \end{aligned}$$

And this result holds for all iterates of $R_{n,a,c}$. □

**Lemma 2.3.** *If $c$ is real and $n \geq 3$, then for every positive integer $k$,*

$$\overline{R^k_{n,\overline{a},c}(\overline{z})} = R^k_{n,a,c}(z).$$

*Proof.* Proving by induction, we establish the base case:

$$\overline{R_{n,\overline{a},c}(\overline{z})} \ = \ \overline{\overline{z}^n + \frac{\overline{a}}{\overline{z}^n} + c} \ = \ \overline{\overline{z^n}} + \overline{\left(\frac{a}{z^n}\right)} + \overline{c} \ = \ z^n + \frac{a}{z^n} + c \ = \ R_{n,a,c}.$$

Now assume the statement is true for $k-1$, then:

$$\begin{aligned} & \overline{R^k_{n,\overline{a},c}(\overline{z})} \\ = \ & \overline{R^{k-1}_{n,\overline{a},c}(R_{n,\overline{a},c}(\overline{z}))} \\ = \ & \overline{R^{k-1}_{n,\overline{a},c}(\overline{R_{n,a,c}(z)})} \ (By\ the\ base\ case) \\ = \ & R^{k-1}_{n,a,c}(R_{n,a,c}(z)) \ (By\ the\ induction\ assumption) \\ = \ & R^k_{n,a,c}(z) \end{aligned}$$

and we have our result by induction. □

**Lemma 2.4.** *If $a$ is real and $n \geq 3$, then for every positive integer $k$,*

$$\overline{R^k_{n,a,\overline{c}}(\overline{z})} = R^k_{n,a,c}(z).$$

*Proof.* Proving by induction, we establish the base case:

$$\overline{R_{n,a,\overline{c}}(\overline{z})} \;=\; \overline{\overline{z}^n + \frac{a}{\overline{z}^n} + \overline{c}} \;=\; \overline{\overline{z^n}} + \frac{a}{\overline{\overline{z^n}}} + \overline{\overline{c}} \;=\; z^n + \frac{a}{z^n} + c \;=\; R_{n,a,c}.$$

Now assume the statement is true for $k-1$, then:

$$\begin{aligned}
& \overline{R^k_{n,a,\overline{c}}(\overline{z})} \\
= \;& \overline{R^{k-1}_{n,a,\overline{c}}(R_{n,a,\overline{c}}(\overline{z}))} \\
= \;& \overline{R^{k-1}_{n,a,\overline{c}}(\overline{R_{n,a,c}(z)})} \; (By\ the\ base\ case) \\
= \;& R^{k-1}_{n,a,c}(R_{n,a,c}(z)) \; (By\ the\ induction\ assumption) \\
= \;& R^k_{n,a,c}(z)
\end{aligned}$$

and we have our result by induction.

□

## 2.2 The Location of Julia Sets of $R_{n,a,c}$

Here we discuss results about the dynamical plane of $R_{n,a,c}$. The paper [HS11] studies the dynamics of $R_{n,a,c}$ and holds a lot of pertinent results, particularly the case of $c$-fixed.

**Lemma 2.5.** *[HS11] For any $c \in \mathbb{C}$ and any $a \in \mathbb{C}$, given any $\epsilon > 0$, there is an $N \geq 2$ such that for all $n \geq N$ the filled Julia set of $R_{n,a,c}$ must lie in the disk of radius $1+\epsilon$ centered at the origin, $\mathbf{D}(0, 1+\epsilon)$.*

This occurs because any point outside $\mathbf{D}(0, 1+\epsilon)$ has an orbit that escapes to $\infty$. We use this result to nail down a specific region where the filled Julia set will lie for $n \geq 3$.

**Lemma 2.6.** *If $n \geq 3$, $|c| \leq 1$, and $\frac{c^2}{4} \leq |a| \leq \left(1 - \frac{c}{2}\right)^2$, then any $|z| > 2$ will lie in $A^*(\infty)$ of $R_{n,a,c}$. Hence, the filled Julia set of $R_{n,a,c}$ lies in the closed disk of radius 2 centered at the origin.*

*Proof.* The proof of Lemma 2.6 in [HS11] says that if $N$ satisfies $(1+\epsilon)^N > 3Max\{1, |a|, |c|\}$ then for $n \geq N$ we have the escape radius of $1 + \epsilon$. That is, the orbits of values $|z| > 1 + \epsilon$ tend to $\infty$. We'll set $\epsilon = 1$, and then by our constraints on $a$ and $c$, we have:

$$3Max\{1, |a|, |c|\} = 3Max\{1, \left(1 - \frac{c}{2}\right)^2, 1\} = 3(2.25) = 6.75$$

for $a$ and $c$ at their greatest moduli. So when we solve this equation for $N$, we find $N > \frac{ln(6.75)}{ln(2)} \approx 2.75$, thus $n \geq 3$ will satisfy the criterion. Because the filled Julia set lies in the complement of $A^*(\infty)$, then the Julia set must lie within a radius of 2 to the origin. □

Combining this with Proposition 2.1 restricts even further where the filled Julia set of $R_{n,a,c}$ will be.

**Lemma 2.7.** *With the same assumptions on $n$, $a$, and $c$ as Lemma 2.6, the filled Julia set of $R_{n,a,c}$ lies within the annulus* $\mathbf{A}\left(\frac{|a|^{\frac{1}{n}}}{2},\ 2\right)$.

*Proof.* Given any $|z| \leq \frac{|a|^{\frac{1}{n}}}{2}$ and the involution symmetry of Proposition 2.1, then $|R_{n,a,c}(z)| \geq 2 \in A^*(\infty)$ and thus these $z$ values also lie in $A(\infty)$. Therefore the filled Julia is a subset of the annulus $\frac{|a|^{\frac{1}{n}}}{2} \leq |z| \leq 2$. □

Figure 2.1 gives an example of a Julia set $R_{n,a,c}$ lying in said annulus. We can see various shapes that appear in this Julia set that look like the Julia set of $P_{-1}$. We shall prove later that these shapes are indeed homeomorphic copies of quadratic Julia sets because $R_{n,a,c}$ is polynomial-like of degree two on those regions.

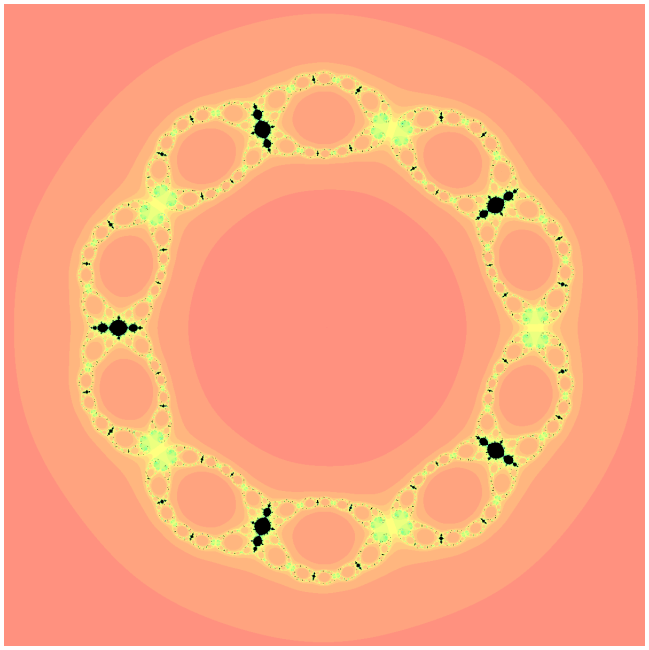

Figure 2.1: Julia set of $R_{n,a,c}$ with $n = 5$, $a = 0.17$, and $c = 0.048$.

## 2.3 $R_{n,a,c}$ is Polynomial-like

Our goal is to show there exist homeomorphic copies of quadratic Julia sets in the dynamical plane of $R_{n,a,c}$ as well as baby $\mathcal{M}$'s in the $a$ and $c$ parameter planes. Achieving this comes by showing that $R_{n,a,c}$ is a polynomial-like map of degree two on small regions. We shall prove this using the same process Devaney used so we first define a subset of the domain of $R_{n,a,c}$:

$$\boxed{\mathbf{U}' = \mathbf{U}'_{n,a} = \left\{ z = re^{i\theta} \;\middle|\; \frac{|a|^{\frac{1}{n}}}{2} < r < 2 \;\; and \;\; \frac{\psi - \pi}{2n} < \theta < \frac{\psi + \pi}{2n} \right\}} \tag{2.1}$$

where $\psi = Arg(a)$, as well as

$$\boxed{\mathbf{U} = \mathbf{U}_{n,c,a} = R_{n,c,a}(\mathbf{U}'_{n,a})}\,. \tag{2.2}$$

A sketch of $\mathbf{U}'$ is given in Figure 2.2. We will show that $R_{n,c,a} : \mathbf{U}' \to \mathbf{U}$ is a family of polynomial-like maps of degree two.

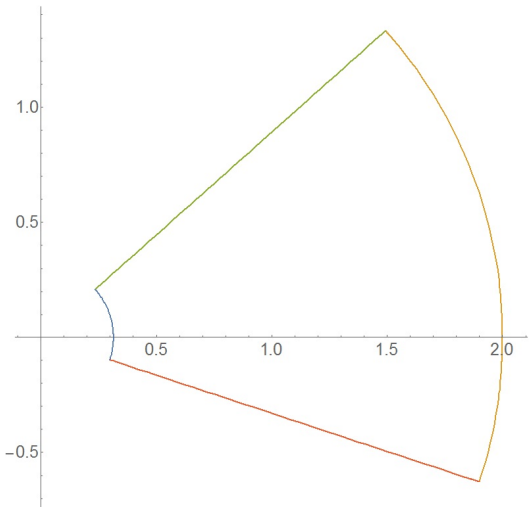


Figure 2.2: A sketch of the set $\mathbf{U}'$ in the dynamical plane of $R_{n,a,c}$

Again the critical points of $R_{n,a,c}$ are $a^{\frac{1}{2n}}$. $\mathbf{U}'$ contains one of these critical points, $|a|^{1/2n}e^{\psi/2n}$, as $\dfrac{|a|^{\frac{1}{n}}}{2} < |a|^{1/2n} < 2$ is true for $|a| < 2^{2n}$. The range of $a$ we work in is well below that threshold. The argument of the critical point, $\dfrac{\psi}{2n}$, is the midpoint of the angular range of $\mathbf{U}'$. The rest of the critical points of $R_{n,a,c}$ are spread out in intervals of $\dfrac{\pi}{n}$ radians and these don't fall within the angular interval of $\left(\dfrac{\psi-\pi}{2n}\ ,\ \dfrac{\psi+\pi}{2n}\right)$. Therefore $\mathbf{U}'$ contains a unique critical point of $R_{n,a,c}$.

Next we show that by this of $\mathbf{U}'$, $\mathbf{U}$ is actually a convenient shape to work with.

**Lemma 2.8.** $\mathbf{U}$ *is half an ellipse centered at* $c$ *and rotated by* $\psi/2$.

*Proof.* Ignoring the restriction on argument, we consider the set

$$\left\{R_{n,c,a}(2e^{i\theta}) \;\middle|\; 0 \le \theta \le 2\pi\right\}.$$

This set contains the image of the outer and inner arcs of $\mathbf{U}'$ by Proposition 2.1. Because we are considering all angles of $\theta$, our set is independent of the starting angle. We can apply an angular shift and the image set will remain the same, thus we instead consider the set

$$\left\{R_{n,c,a}(2e^{i\left(\theta+\frac{\psi}{2n}\right)}) \;\middle|\; 0 \le \theta \le 2\pi\right\}.$$

So

$$
\begin{aligned}
& R_{n,c,a}\left(2e^{i\left(\theta+\frac{\psi}{2n}\right)}\right) \qquad (2.3)\\
= & \left(2*\exp\left(i\left(\theta+\frac{\psi}{2n}\right)\right)\right)^n+\frac{a}{\left(2*\exp\left(i\left(\theta+\frac{\psi}{2n}\right)\right)\right)^n}+c\\
= & 2^n*\exp\left(i\left(n\theta+\frac{\psi}{2}\right)\right)+\frac{|a|e^{i\psi}}{2^n*\exp\left(i\left(n\theta+\frac{\psi}{2}\right)\right)}+c\\
= & 2^n*\exp\left(i\left(n\theta+\frac{\psi}{2}\right)\right)+\frac{|a|}{2^n}*\exp\left(i\left(\psi-\left(n\theta+\frac{\psi}{2}\right)\right)\right)+c\\
= & e^{i\frac{\psi}{2}}\left(2^n e^{in\theta}+\frac{|a|}{2^n}e^{-in\theta}\right)+c\\
= & e^{i\frac{\psi}{2}}\left(2^n\left(\cos\left(n\theta\right)+i\sin\left(n\theta\right)\right)+\frac{|a|}{2^n}\left(\cos\left(n\theta\right)-i\sin\left(n\theta\right)\right)\right)+c. \qquad (2.4)
\end{aligned}
$$

From this we focus further on:

$$
\begin{aligned}
& 2^n(\cos(n\theta)+i\sin(n\theta))+\frac{|a|}{2^n}(\cos(n\theta)-i\sin(n\theta))\\
& \quad =\left(2^n+\frac{|a|}{2^n}\right)\cos(n\theta)+i\left(2^n-\frac{|a|}{2^n}\right)\sin(n\theta).
\end{aligned}
$$

So defined parametrically, we have:

$$
\begin{aligned}
x= & \left(2^n+\tfrac{|a|}{2^n}\right)\cos(n\theta)\\
y= & \left(2^n-\tfrac{|a|}{2^n}\right)\sin(n\theta).
\end{aligned} \qquad (2.5)
$$

Compare this to the parametric equation of an ellipse centered at the origin:

$$
\begin{aligned}
x= & \; b\cos(\phi)\\
y= & \; d\sin(\phi)
\end{aligned}
$$

where $0\leq\phi\leq 2\pi$, $b$ is half the length of the major axis along the x-axis, and $d$ is half the length of the minor axis along the y-axis.

Thus the equation set (2.5) is an ellipse centered at the origin with a major axis length

of $2\left(2^n + \frac{|a|}{2^n}\right)$, and a minor axis length $2\left(2^n - \frac{|a|}{2^n}\right)$ that wraps around $n$ times. Going back to (2.4) we find our image set to be the ellipse described above, rotated by $\psi/2$ and centered at $c$. By our independence of starting angle, this gives us equality to the first set described, and $\left\{R_{n,c,a}(2e^{i\theta}) \;\middle|\; 0 \le \theta \le 2\pi\right\}$ is this exact ellipse as well. Thus we define

$$\boxed{\mathcal{E} = R_{n,c,a}\left(2e^{i\theta}\right) = \left\{ \begin{array}{rl} x = & \left(2^n + \frac{|a|}{2^n}\right)\cos(n\theta) \\ y = & \left(2^n - \frac{|a|}{2^n}\right)\sin(n\theta) \end{array} \right\}}. \tag{2.6}$$

Now we look at the image of the rays $re^{i\frac{\psi\pm\pi}{2n}}$ for $\frac{|a|^{\frac{1}{n}}}{2} < \; r \; < 2$.

$$\begin{aligned} R_{n,c,a}(re^{i\frac{\psi\pm\pi}{2n}}) &= \left(r * \exp\left(i\frac{\psi\pm\pi}{2n}\right)\right)^n + \frac{a}{\left(r * \exp\left(i\frac{\psi\pm\pi}{2n}\right)\right)^n} + c \\ &= r^n * \exp\left(i\frac{\psi\pm\pi}{2}\right) + \frac{|a|e^{i\psi}}{r^n * \exp\left(i\frac{\psi\pm\pi}{2}\right)} + c \\ &= r^n * \exp\left(i\frac{\psi\pm\pi}{2}\right) + \frac{|a|}{r^n} * \exp\left(i\frac{\psi\mp\pi}{2}\right) + c \\ &= \exp\left(i\frac{\psi}{2}\right)\left(r^n * \exp\left(\pm i\frac{\pi}{2}\right) + \frac{|a|}{r^n} * \exp\left(\mp i\frac{\pi}{2}\right)\right) + c \\ &= \pm e^{i\frac{\psi}{2}}\left(r^n - \frac{|a|}{r^n}\right)i + c. \end{aligned}$$

This is a line segment on the imaginary axis from $-\left(2^n - \frac{|a|}{2^n}\right)i$ to $\left(2^n - \frac{|a|}{2^n}\right)i$, rotated by $\psi/2$, then shifted by $c$. In fact, this is actually the minor axis of $\mathcal{E}$.

Finally we investigate the original restriction of $\theta$,

$$\frac{\psi - \pi}{2n} < \; \theta \; < \frac{\psi + \pi}{2n},$$

and find that (2.5) gives us

$$\frac{\psi}{2} - \frac{\pi}{2} < n\theta < \frac{\psi}{2} + \frac{\pi}{2}.$$

We see the angular range is $\pi$ radians in size, hence yielding half an ellipse. Combine this

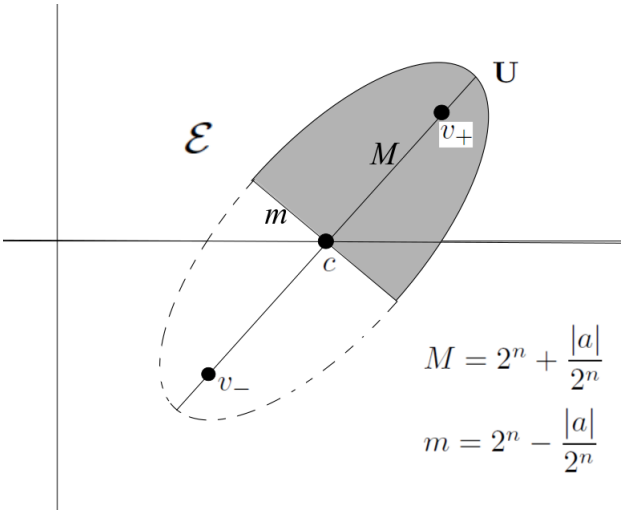


Figure 2.3: A sketch of **U**. It is a half ellipse cut by the minor axis centered at $c$ and rotated by $\frac{\psi}{2}$

curve with the minor axis of $\mathcal{E}$ (the image of the rays) and we have that **U** is a half ellipse rotated by $\psi/2$ and centered at $c$. (See Figure 2.3) □

Knowing that **U** is half an ellipse gives a more simple way to describe the image of $\mathbf{U}'$ and how it is affected by changes in $n$, $a$, and $c$.

**Lemma 2.9.** *$v_\pm$ are the foci of $\mathcal{E}$.*

*Proof.* For any ellipse, the foci lie on the major axis. The square of the distance of a focal point from the center is equal to difference of the squares of half the major and minor axis lengths. So we get:

$$\sqrt{\left(2^n + \frac{a}{2^n}\right)^2 - \left(2^n - \frac{a}{2^n}\right)^2} = \sqrt{4a} = 2\sqrt{a}.$$

Since the center of $\mathcal{E}$ is $c$, the foci of $\mathcal{E}$ must be $c \pm 2\sqrt{a} = v_\pm$. □

Using Lemma 2.9 we can describe $\mathcal{E}$ with another equation,

$$\boxed{\mathcal{E} = \left\{ z \;\middle|\; |z - v_-| + |z - v_+| = 2^{n+1} + \frac{|a|}{2^{n-1}} \right\}}. \tag{2.7}$$

### 2.3.1

In this subsection we show $R_{n,a,c}$ is polynomial-like of degree two (Proposition 2.12) with the restrictions of $\frac{c^2}{4} \leq \ |a| \ \leq \left(1-\frac{c}{2}\right)^2$, and $|c| \leq 1$. First we show $\mathbf{U}'$ is contained in $\mathcal{E}$, then we will go further from there to show $\mathbf{U}' \subset \mathbf{U}$.

**Lemma 2.10.** *Given $n \geq 3$, $\frac{c^2}{4} \leq \ |a| \ \leq \left(1-\frac{c}{2}\right)^2$, and $|c| \leq 1$ then $\mathbf{U}' \subseteq \mathcal{E}$.*

*Proof.* Since $\mathbf{U}' \subseteq \overline{\mathbf{D}(0,2)}$ we will assume $|z| \leq 2$ and prove $\overline{\mathbf{D}(0,2)} \subseteq \mathcal{E}$, and thus $\mathbf{U}' \subseteq \mathcal{E}$.

So

$$\begin{aligned}
& |z-v_-| + |z-v_+| \\
= \ & |z-(c-2\sqrt{a})| + |z-(c+2\sqrt{a})| \\
\leq \ & 2|z| + 2|c| + 4\sqrt{|a|} \\
\leq \ & 2(2) + 2(1) + 4\sqrt{\left(1-\frac{c}{2}\right)^2} \\
\leq \ & 4 + 2 + 4(1.5) \\
< \ & 16 \\
(\textit{since } n \geq 3) \ \leq \ & 2^{n+1} \ \leq \ 2^{n+1} + \frac{|a|}{2^{n-1}}.
\end{aligned}$$

By Lemma 2.9 and the description of $\mathcal{E}$ in Equation (2.7), these inequalities yield that $\mathbf{U}' \subseteq \mathcal{E}$ under the restrictions on $|a|$ and $|c|$. □

Having $\mathbf{U}'$ contained in $\mathcal{E}$ is one thing but we need to restrict further to one half of $\mathcal{E}$. The critical point in $\mathbf{U}'$ maps to $v_+$ which is in the right half of $\mathcal{E}$. We will restrict the argument of $a$ to $|\psi| \ \leq \frac{\pi}{n-1}$ which is bounded by $\frac{\pi}{2}$ for $n \geq 3$. Since $\mathcal{E}$ is a horizontal ellipse rotated by $\frac{\psi}{2}$, then under this restriction $\mathcal{E}$ is rotated by $\frac{\pi}{4}$ at most. In our next lemma we give criterion for which the minor axis of $\mathcal{E}$ does not intersect $\mathbf{U}'$ and at worst intersects $\partial\overline{\mathbf{U}'}$ on the left side. This will then give us that $\mathbf{U}' \subset \mathbf{U}$.

**Lemma 2.11.** *For $n \geq 3$ and real $c < \frac{|a|^{\frac{1}{n}}}{2\sqrt{2}}$, the minor axis of $\mathcal{E}$ does not intersect $\mathbf{U}'$.*

*Proof.* Keeping the restriction to the argument of $a$, $|\psi| \leq \frac{\pi}{2}$, we determine the value of $c$ for which the minor axis intersects $\mathbf{U}'$ when $\psi = \pm\frac{\pi}{2}$.

Based on Figure 2.4a, if we start with $\psi = \frac{\pi}{2}$ then the minor axis will be rotated by $\frac{\pi}{4}$ with respect to the imaginary-axis and then shifted by $c$. We shall determine the value of $c$ for which the minor axis hits the lower left vertex of $\mathbf{U}'$ at modulus $\frac{|a|^{\frac{1}{n}}}{2}$ and argument $\frac{\frac{\pi}{2} - \pi}{2n} = -\frac{\pi}{4n}$. The coordinates of this intersection point are

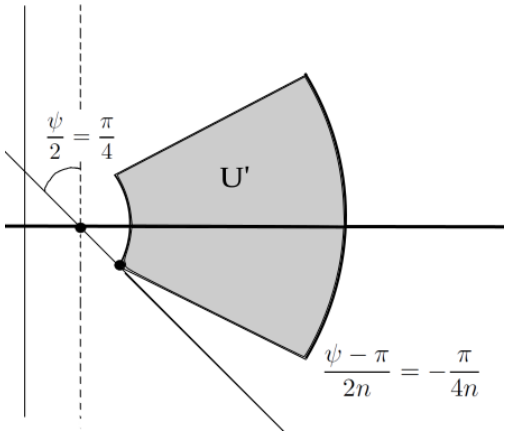


(a) The minor axis of $\mathcal{E}$ intersecting $\partial\mathbf{U}'$.

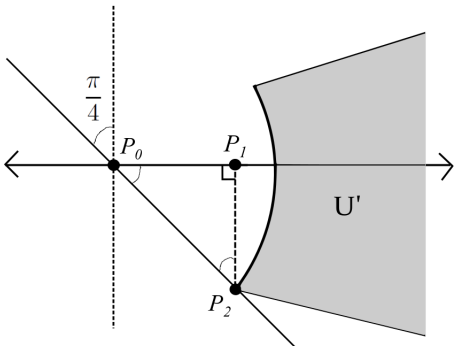


(b) A closer zoom in on the point where the minor axis of $\mathcal{E}$ intersects the 'corner' of $\mathbf{U}'$.

$P_2 = \left(\frac{|a|^{\frac{1}{n}}}{2}\cos\left(\frac{\pi}{4n}\right) \ , \ -\frac{|a|^{\frac{1}{n}}}{2}\sin\left(\frac{\pi}{4n}\right)\right)$. With a closer view, we have a right triangle setup as shown in Figure 2.4b and because $\frac{\psi}{2} = \frac{\pi}{4}$, both legs of the triangle are equal length. The coordinates of the other two points of the triangle are $P_0 = (0, c)$ and $P_1 = \left(\frac{|a|^{\frac{1}{n}}}{2}\cos\left(\frac{\pi}{4n}\right) \ , \ 0\right)$. The length of the vertical leg is the absolute value of the imaginary component of $P_2$. The length of the horizontal leg is the difference between the real components of $P_0$ and $P_1$. We set these values equal to each other:

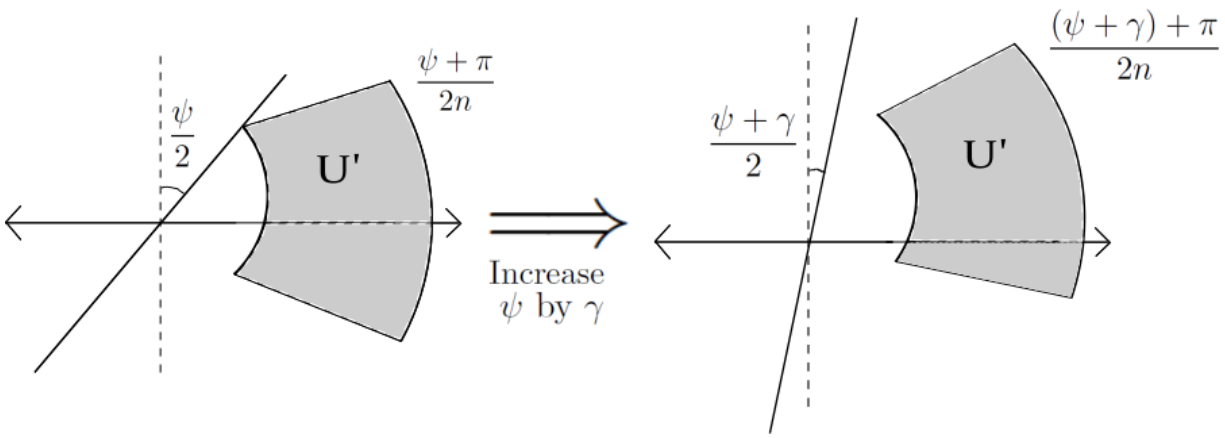


Figure 2.5: Increasing the angle shows no intersection of the axis.

$$\begin{aligned}
\frac{|a|^{\frac{1}{n}}}{2}\sin\left(\frac{\pi}{4n}\right) &= \frac{|a|^{\frac{1}{n}}}{2}\cos\left(\frac{\pi}{4n}\right) - c \\
\Rightarrow c &= \frac{|a|^{\frac{1}{n}}}{2}\left(\cos\left(\frac{\pi}{4n}\right) - \sin\left(\frac{\pi}{4n}\right)\right) \\
&\geq \frac{|a|^{\frac{1}{n}}}{2}\left(\cos\left(\frac{\pi}{12}\right) - \sin\left(\frac{\pi}{12}\right)\right) \ (\textit{Since } n \geq 3) \\
&= \frac{|a|^{\frac{1}{n}}}{2\sqrt{2}}.
\end{aligned}$$

Thus the smallest $c$ value for which the minor axis of $\mathcal{E}$ intersects $\mathbf{U}'$ is $c = \frac{|a|^{\frac{1}{n}}}{2\sqrt{2}}$, so choosing $-1 \leq c < \frac{|a|^{\frac{1}{n}}}{2\sqrt{2}}$ gives that $\mathbf{U}' \cap \mathbf{U} = \emptyset$.

Now if we go to the other extreme and let $\psi = -\frac{\pi}{2}$ the work will be just the same.

Here our intersection point is now $\left(\frac{|a|^{\frac{1}{n}}}{2}\cos\left(\frac{\pi}{4n}\right),\ \frac{|a|^{\frac{1}{n}}}{2}\sin\left(\frac{\pi}{4n}\right)\right)$, and the triangle is just a reflection of the previous case across the real axis. Therefore our result is the same as above.

Lastly we argue that for $c = \frac{|a|^{\frac{1}{n}}}{2\sqrt{2}}$, the minor axis will only touch the corners of $\mathbf{U}'$ at $\psi = \pm\frac{\pi}{2}$ and there will be no intersection for any $\psi$ or $c$ value smaller than these bounds.

When we change $\psi$, the overall change in angle of the minor axis will be larger than the

overall change in angle of the rays of $\mathbf{U}'$. Starting at $\psi = -\frac{\pi}{2}$ and increasing by some value $\gamma$, we find the change in angle of the minor axis to be

$$\frac{\psi + \gamma}{2} - \frac{\psi}{2} = \frac{\gamma}{2}$$

and the change in angle of the upper ray of $\mathbf{U}'$ to be

$$\frac{(\psi + \gamma) + \pi}{2n} - \frac{\psi + \pi}{2n} = \frac{\gamma}{2n}.$$

Since $n \geq 3$, then $\frac{\gamma}{2} > \frac{\gamma}{2n}$ and the minor axis won't touch $\mathbf{U}'$ again until it goes too far and hits the "lower left" corner of $\mathbf{U}'$. As shown above though, this won't occur until $\psi = \frac{\pi}{2}$.

Therefore for $c < \frac{|a|^{\frac{1}{n}}}{2\sqrt{2}}$ we find the minor axis of $\mathcal{E}$ will not intersect $\mathbf{U}'$. □

Figure 2.6 gives one example of $\mathbf{U}' \subset \mathbf{U}$. Now we can show that $R_{n,a,c}$ is polynomial-like on $\mathbf{U}'$.

**Proposition 2.12.** *$R_{n,a,c} : \mathbf{U}' \to \mathbf{U}$ is polynomial-like of degree two when $n \geq 3$, $\frac{c^2}{4} \leq |a| \leq \left(1 - \frac{c}{2}\right)^2$, and $-1 \leq c \leq 0$.*

*Proof.* $\mathbf{U}'$ and $\mathbf{U}$ are bounded, open, and simply connected. Combining the results from Lemma 2.10 and Lemma 2.11 along with restriction that $-1 \leq c \leq 0 < \frac{|a|^{\frac{1}{n}}}{2\sqrt{2}}$ yields that $\mathbf{U}' \subset \mathbf{U}$. Also using Proposition 2.1 and the fact that $\mathbf{U}'$ contains a unique critical point shows that $R_{n,a,c}$ is a two-to-one map on $\mathbf{U}'$.

Lastly $R_{n,a,c}$ is analytic on $\mathbf{U}'$ as $a \neq 0$ and $\mathbf{U}'$ does not contain the origin. Therefore the family $R_{n,a,c}$ is polynomial-like of degree two for the given restrictions on $n$, $a$, and $c$. □

Now because of the polynomial-like behavior of $R_{n,a,c}$, we see the reason for baby quadratic Julia sets appearing in the dynamical plane of $R_{n,a,c}$.

**Corollary 2.13.** *With the same assumptions on $n$, $a$, and $c$ as Proposition 2.12, the set of values in $\mathbf{U}'$ whose orbits do not escape $\mathbf{U}'$ is homeomorphic to a quadratic filled Julia set.*

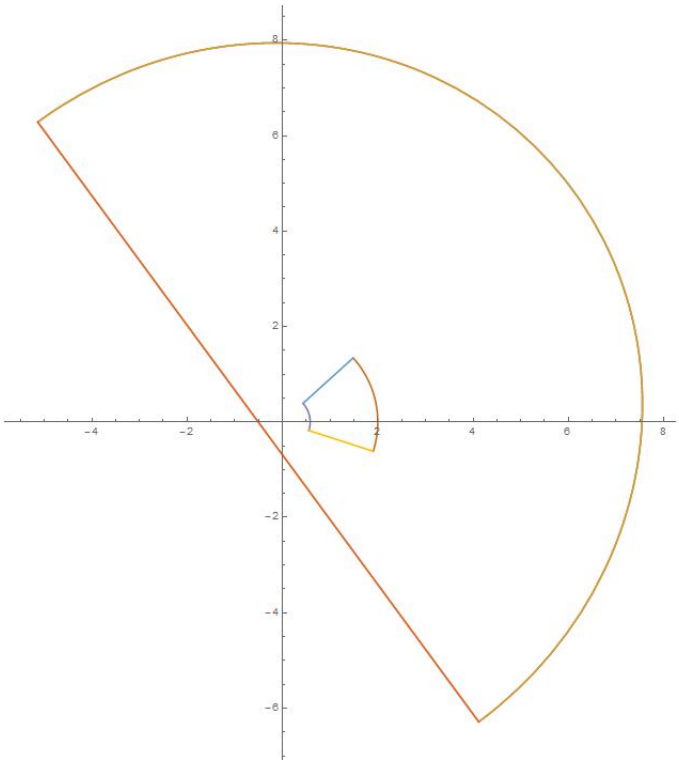


Figure 2.6: An example of $\mathbf{U}'$ sitting inside $\mathbf{U}$.

*Proof.* Having established that $R_{n,a,c}$ is polynomial like of the degree two in Proposition 2.12, then by Theorem 1.3 $R_{n,a,c}$ is topologically conjugate to some quadratic polynomial on that polynomial's filled Julia set. This polynomial's Julia set is the baby Julia set we find in the dynamical plane of $R_{n,a,c}$. □

Figure 2.7 gives examples of these baby basilica Julia sets occurring in the dynamical plane of $R_{n,a,c}$.

### 2.3.2

In this subsection we repeat the process to show that $R_{n,a,c}$ is polynomial-like for different criterion on the parameters:

$$1 \leq a \leq \frac{(2^{n+1}-8)^2}{16}, \ c \textit{ such that } |v_+| \leq 2.$$

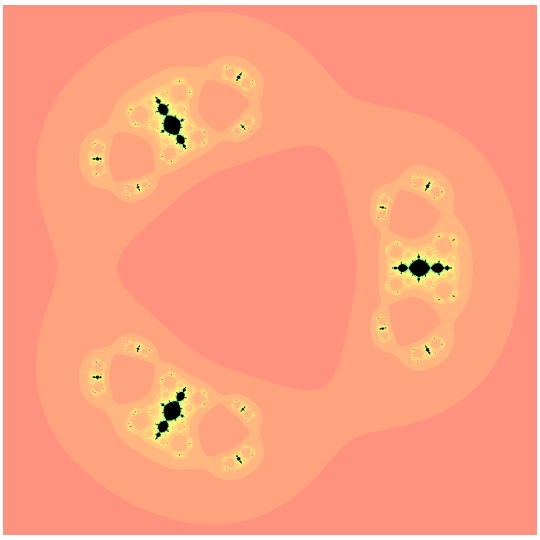

Figure 2.7: Dynamical Plane of $R_{n,a,c}$ with $n = 3$, $a = 0.88$, and $c = -1$. Note the baby basilicas.

The restrictions on $c$ in this case come from the fact that we will trace the critical value $v_+$ around the boundary of $\mathbf{U}'$ following the methods of Douady and Hubbard. That will be used later, but first we show $\mathbf{U}' \subset \mathbf{U}$ for the first requirements of a polynomial-like map.

**Lemma 2.14.** *Let $n \geq 3$, $a$ real and satisfying $1 \leq a \leq \dfrac{(2^{n+1}-8)^2}{16}$ and $c$ satisfies $|v_+| \leq 2$. With the same definitions for $\mathbf{U}'$ and $\mathcal{E}$ as above, then $\mathbf{U}' \subset \mathcal{E}$.*

*Proof.* We start with the critical value $|v_+| = 2$ at its largest modulus so we have the equation

$$c + 2\sqrt{a} = 2e^{i\theta},\ \theta \in [0, 2\pi).$$

Solving for $c$ gets us $c = 2e^{i\theta} - 2\sqrt{a}$ and we attain bounds for $v_-$ as well:

$$\begin{aligned} & |v_+| = 2 \\ \Rightarrow \quad & |v_-| = |c - 2\sqrt{a}| = |(2e^{i\theta} - 2\sqrt{a}) - 2\sqrt{a}| = \sqrt{4 + 16a - 16\cos(\theta)\sqrt{a}}. \end{aligned}$$

To find the largest value of $|v_-|$, we take a derivative with respect to $\theta$:

$$\frac{8\sqrt{a}\sin(\theta)}{\sqrt{4+16a-16\cos(\theta)\sqrt{a}}}.$$

This means $|v_-|$ has critical points at $\theta = \{0, \pi\} \in [0, 2\pi)$. By the second derivative test, $\theta = \pi$ gives us a max modulus of $2 + 4\sqrt{a}$.

We shall prove again that $\overline{\mathbf{D}(0,2)} \subseteq \mathcal{E}$, and thus $\mathbf{U}' \subseteq \mathcal{E}$. Using the facts that $|z| \leq 2$, $|c + 2\sqrt{a}| \leq 2$ and $|c - 2\sqrt{a}| \leq 2 + 4\sqrt{a}$ we find

$$\begin{aligned}
& |z - v_-| + |z - v_+| \\
= \; & |z - (c - 2\sqrt{a})| + |z - (c + 2\sqrt{a})| \\
\leq \; & 2|z| + |c + 2\sqrt{a}| + |c - 2\sqrt{a}| \\
\leq \; & 4 + (2) + (2 + 4\sqrt{a}) \\
= \; & 8 + 4\sqrt{a} \\
\leq \; & 8 + 4\sqrt{\frac{(2^{n+1} - 8)^2}{16}} \\
= \; & 8 + 4\frac{(2^{n+1} - 8)}{4} \\
= \; & 2^{n+1} \leq \; 2^{n+1} + \frac{|a|}{2^{n-1}}.
\end{aligned}$$

Thus by Equation (2.7), we find $\mathbf{U}' \subset \mathcal{E}$. □

Continuing further, we show that the minor axis of $\mathcal{E}$ does not intersect $\mathbf{U}'$.

**Lemma 2.15.** *Under the same hypotheses on n, a, and c as Lemma 2.14,*

$\mathbf{U}' \subset R_{n,a,c}(\mathbf{U}') = \mathbf{U}$.

*Proof.* Just like the proof of 2.11, all we need to show is that the minor axis of $\mathcal{E}$ does not cross $\mathbf{U}'$. As seen earlier, the minor axis of $\mathcal{E}$ is a line through $c$ rotated by $\frac{Arg(a)}{2} = 0$ making the minor axis a vertical line. Thus the value of $Re(c)$ determines the location of the minor axis. In the proof of 2.14 we found for the critical value at its greatest modulus

of $|v_+| = 2$ that $c = 2e^{i\theta} - 2\sqrt{a}$. Therefore

$$Re(c) = 2\cos(\theta) - 2\sqrt{a} \leq 2 - 2 = 0$$

since $a \geq 1$. Thus if $Re(c)$ is non-positive, then the minor axis of $\mathcal{E}$ is never in the right half dynamical plane.

Since $Arg(a) = 0$ and $n \geq 3$, then the complex arguments of values lying in $\mathbf{U}'$ lie between $\pm\frac{\pi}{6}$ which gives that $\mathbf{U}'$ lies completely in the right half complex plane. Therefore the minor axis of $\mathcal{E}$ will never intersect $\mathbf{U}'$ under these conditions and $\mathbf{U}' \subset \mathbf{U}$. □

These two Lemmas form the key to the next result.

**Proposition 2.16.** *For $n \geq 3$, $1 \leq a \leq \dfrac{(2^{n+1}-8)^2}{16}$ and $c$ such that $|v_+| \leq 2$, $R_{n,a,c} : \mathbf{U}' \to \mathbf{U}$ is polynomial-like of degree two.*

*Proof.* Similiar to Proposition 2.12 we find that $R_{n,a,c} : \mathbf{U}' \to \mathbf{U}$ satisfies the definition of a degree two polynomial-like map by being analytic on $\mathbf{U}'$ and $\mathbf{U}' \subset \mathbf{U}$ by Lemma 2.15. □

With this, we have another result on the existence of baby quadratic Julia sets occurring in the dynamical plane of $R_{n,a,c}$ (refer to Figure 2.8 for an example of baby rabbit Julia sets). The proof is omitted as it is the exact same as the proof to Corollary 2.13 using Proposition 2.16.

**Corollary 2.17.** *With the same assumptions as Proposition 2.16, the set of values in $\mathbf{U}'$ whose orbits do not escape $\mathbf{U}'$ is homeomorphic to a quadratic filled Julia set.*

Knowing that $R_{n,a,c}$ is polynomial-like of degree two lays the groundwork for the existence of baby $\mathcal{M}$'s in the parameter planes. This will require families of polynomial-like maps as described in Theorem 1.4. The next chapter proves the main results of Theorems 3.3 and 3.12.

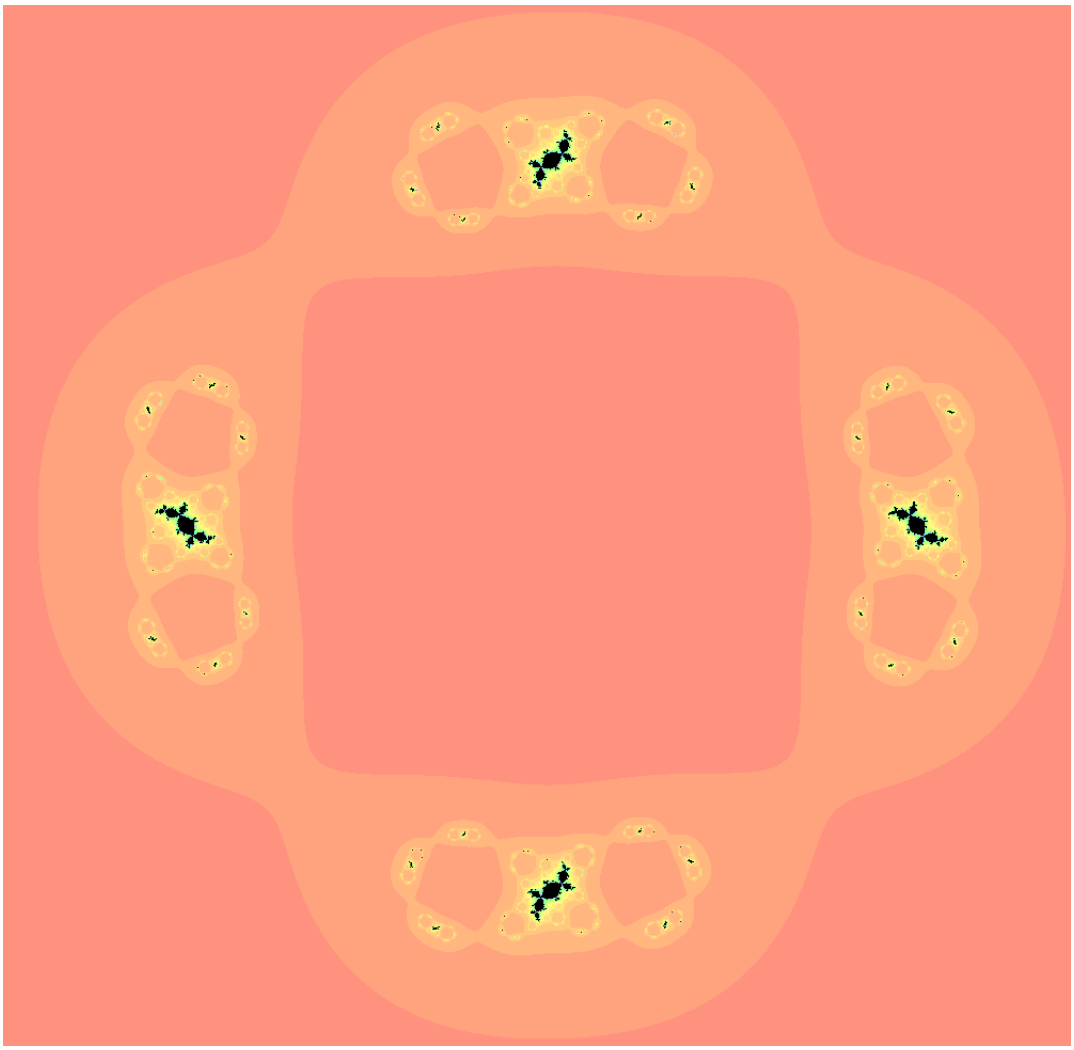

Figure 2.8: The dynamical plane of $R_{n,a,c}$ with $n = 4$, $a = 1$, and $c = -1.01 + 0.046$. Note the baby rabbits.

# Chapter 3

# Parameter Planes of $R_{n,a,c}$

We now focus on the parameter planes of $R_{n,a,c}$. Our first case will be to keep $c$ fixed and let $a$ vary. There are a few results about the $a$-parameter plane that we will extend upon. The second section is new territory where we switch the constant parameter and study the $c$-parameter plane. There are similarities between the two cases but also unexpected differences.

## 3.1 Case: $c$ Fixed and Real

We start with a quick discussion on the multiple critical orbits of $R_{n,a,c}$. We have to be more specific when referring to the 'boundedness locus' of $R_{n,a,c}$ so we define $\mathbb{M}_{n,c}$ ($\mathbb{M}_{n,a}$) as the set of $a$ ($c$) values for which at least one of the critical orbits are bounded. More precisely we define $\mathbb{M}^{\pm}_{n,c}$ as the sets of $a$-values for which the critical orbit of $v_{\pm}$ is bounded respectively, and similarly define $\mathbb{M}^{\pm}_{n,a}$ as the set of $c$-values for which the critical orbit of $v_{\pm}$ is bounded respectively.

In [HS11] it is shown that the conditions for both critical orbits to be bounded in the $a$-parameter plane are tight.

**Proposition 3.1.** *[HS11] If $|c| > 1$, then there is an $N \geq 2$ such that for all $n \geq N$,*

$\mathbb{M}^+_{n,c} \cap \mathbb{M}^-_{n,c} = \emptyset$. *That is at most one critical orbit is bounded in the a-parameter plane for* $|c| > 1$.

In light of this proposition we shall assume $|c| \leq 1$ for the rest of this section. This goes along with results from Chapter 2 that will be used here but small values of $c$ also make for interesting dynamics of $R_{n,a,c}$ that will be discussed more in Chapter 4.

Further results in [HS11] show that as $n$ tends to $\infty$, the Julia set (as well as the filled Julia set) of $R_{n,a,c}$ limit to the unit circle. It is also shown that $\mathbb{M}_{n,c}$ tends to a polar limaçon $r = \dfrac{c + \cos(\theta)}{2}$ shifted by $\dfrac{c^2 - 1}{4}$ as $n \to \infty$.

To draw an $a$-parameter plane of $R_{n,a,c}$ we first fix a value of $c$, then observe the behavior of both critical orbits for every $a$ value. We assign two colors (one for each critical orbit) to each value as follows:

- If the critical orbit is bounded, assign black to that $a$ value.
- If the critical orbit escapes, assign a color like purple or green, dependent on which critical orbit, to that $a$ value. The shade of the color depends on how fast the critical orbit escaped.

For each $a$ value, once two RGB values are assigned, the computer averages them, and the resultant RGB value is the color we see. Figure 3.1 gives a few examples of $a$-parameter planes for a couple $c$-values. This same process will be replicated when we draw a $c$-parameter plane.

To prove the existence of baby $\mathcal{M}$'s in an $a$-parameter plane we look to satisfy the hypotheses of Theorem 1.4. Proposition 2.12 showed that $R_{n,a,c}$ is a polynomial-like map of degree two for $n \geq 3$, $\dfrac{c^2}{4} \leq |a| \leq \left(1 - \dfrac{c}{2}\right)^2$, and $-1 \leq c \leq 0$. $R_{n,a,c}$ is also holomorphic on $\mathbf{U}'$ in $a$ and $z$ as we avoid any poles. Below, we define a set $\mathbf{W}_{n,c}$ to satisfy the remaining hypotheses of Theorem 1.4 and show that $v_+$ takes a closed loop around $\mathbf{U} - \mathbf{U}'$ as $a$ loops around $\partial\mathbf{W}_{n,c}$.

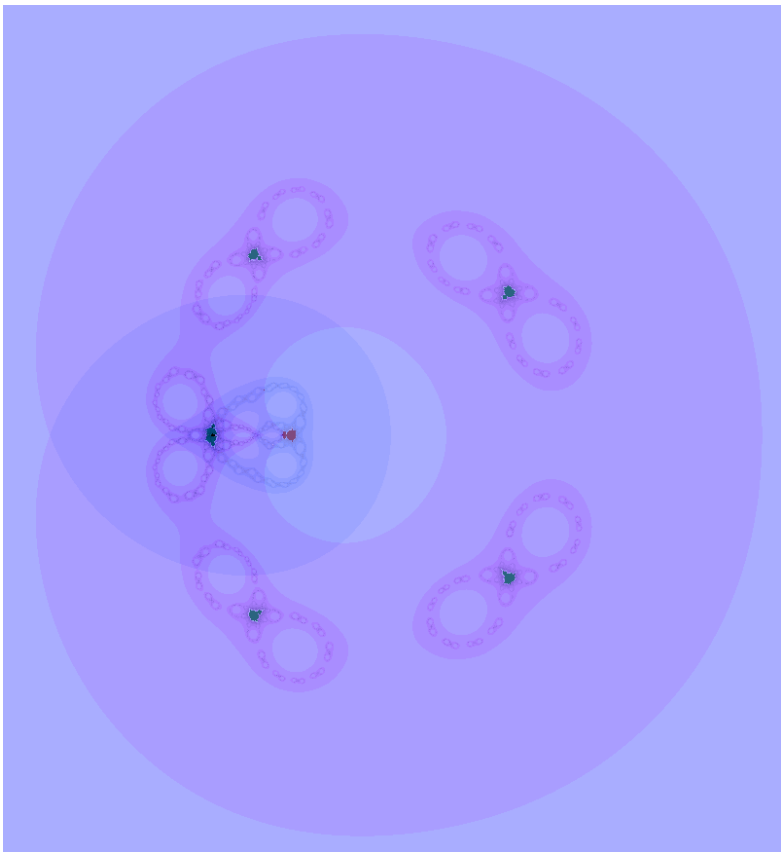

(a) $a$-parameter plane of $R_{n,a,c}$ for $n = 8$ and $c = 0.5$.

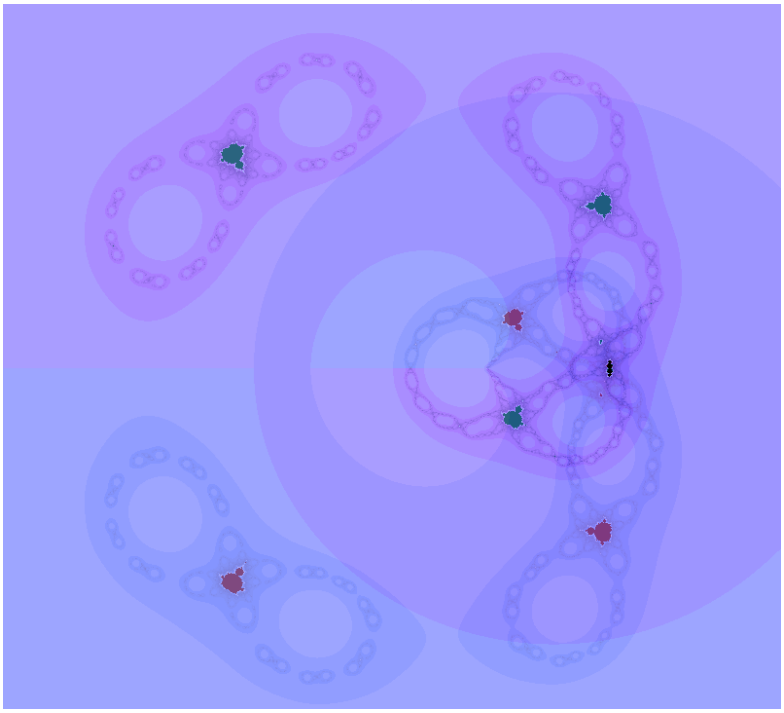

(b) $a$-parameter plane of $R_{n,a,c}$ for $n = 7$ and $c = 0.4i$.

Figure 3.1: $\mathbb{M}_{n,c}$ lying along a limaçon.

$$\boxed{\mathbf{W}_{n,c} = \left\{ a \;\middle|\; \frac{c^2}{4} \leq \; |a| \; \leq \left(1 - \frac{c}{2}\right)^2 \;\; and \;\; |\psi| \leq \frac{\pi}{n-1} \right\}}. \tag{3.1}$$

**Proposition 3.2.** *For $n \geq 3$ and $-1 \leq c \leq 0$, as $a$ travels around $\partial \mathbf{W}_{n,c}$, $v_+$ loops around $\mathbf{U} - \mathbf{U}'$.*

*Proof.* We start with $|a| = \dfrac{c^2}{4}$ on the inside arc of $\mathbf{W}_{n,c}$. Here

$$Re(v_+) = Re\left(c + 2\sqrt{a}\right) = c + 2\sqrt{|a|}\cos\left(\frac{\psi}{2}\right) = c + |c|\cos\left(\frac{\psi}{2}\right) \leq c + |c| = 0$$

since $c \leq 0$. This means $v_+$ never lies in the right half plane. The inside arc of $\mathbf{U}'$ is always in the right half plane because

$$|Arg(z \in \mathbf{U}')| \leq \left| \frac{\pm\frac{\pi}{n-1} \pm \pi}{2n} \right| \leq \frac{\pi}{2(n-1)} < \frac{\pi}{2}$$

for $|Arg(a)| \leq \dfrac{\pi}{n-1}$ and $n \geq 3$. This means that $v_+$ lies to the left of $\mathbf{U}'$ when $a$ is on the inside arc of $\mathbf{W}_{n,c}$.

Now for $a$ on the upper ray of $\mathbf{W}_{n,c}$, we see $Arg(a) = \dfrac{\pi}{n-1}$ and thus $Arg(z \in \mathbf{U}') = \dfrac{\pi}{2(n-1)}$. Because $c$ is real and non-positive, we find

$$\begin{aligned} Arg(v_+) &= Arg(c + 2\sqrt{a}) \\ &\geq Arg(2\sqrt{a}) \\ &= \frac{\psi}{2} \\ &= \frac{1}{2}\frac{\pi}{n-1} \\ &= Arg(z \in \mathbf{U}'). \end{aligned}$$

So at worst $v_+$ touches the upper ray of $\mathbf{U}'$ when $a$ is on the upper ray of $\mathbf{W}_{n,c}$. This is permissible as $\mathbf{U}'$ is open.

When we reach the outer arc of $\mathbf{W}_{n,c}$ where $|a| = \left(1 - \frac{c}{2}\right)^2$, we find that

$$|v_+| = |c + 2\sqrt{a}| = \sqrt{c^2 + 4|a| + 4c\sqrt{|a|}\cos\left(\frac{\psi}{2}\right)} = \sqrt{4 - 4c + 2c^2 - 2c(c-2)\cos\left(\frac{\psi}{2}\right)}.$$

To find the minimum of this, we take a derivative with respect to $\psi$ and get

$$\frac{c(c-2)\sin\left(\frac{\psi}{2}\right)}{2\sqrt{4 - 4c + 2c^2 - 2c(c-2)\cos\left(\frac{\psi}{2}\right)}},$$

and the modulus has a critical point at $\psi = 0$. Using the second derivative test we find a minimum occurs at $\psi = 0$, and evaluating the modulus at $\psi = 0$ gives

$$|v_+| = \sqrt{4 - 4c + 2c^2 - 2c(c-2)(1)} = 2.$$

Therefore, at worst $v_+$ just touches the outer boundary arc of $\mathbf{U}'$ as $a$ travels along the outer arc of $\mathbf{W}_{n,c}$ (still permissible with $\mathbf{U}'$ open).

Now for $a$ on the lower ray, $Arg(a) = -\dfrac{\pi}{n-1}$. Using this and the fact that $Arg(c) = -\pi$, we find

$$Arg(z \in \mathbf{U}') > -\frac{1}{2}\frac{\pi}{n-1} = Arg(2\sqrt{a}) \geq Arg(c + 2\sqrt{a}).$$

So $Arg(z \in \mathbf{U}') > Arg(v_+)$ for all $a$ on the lower ray of $\mathbf{W}_{n,c}$ and $v_+$ lies below $\mathbf{U}'$.

Therefore as $a$ comes back to its starting position in $\partial\mathbf{W}_{n,c}$, $v_+$ has finished a closed loop around the outside of $\mathbf{U}'$. □

**Theorem 3.3.** *For $n \geq 3$ and $-1 \leq c \leq 0$, the set of $a$-values within $\mathbf{W}_{n,c}$ for which the orbit of $v_+$ does not escape $\mathbf{U}'$ is homeomorphic to $\mathcal{M}$.*

*Proof.* With Propositions 2.12 and 3.2 we satisfy the necessary conditions of Theorem 1.4 for the existence of a baby $\mathcal{M}$ lying in $\mathbf{W}_{n,c}$. □

We have the existence of our first baby $\mathcal{M}$ in $\mathbb{M}^+_{n,c}$, and Figure 3.2 gives an example of one lying in $\mathbf{W}_{n,c}$.

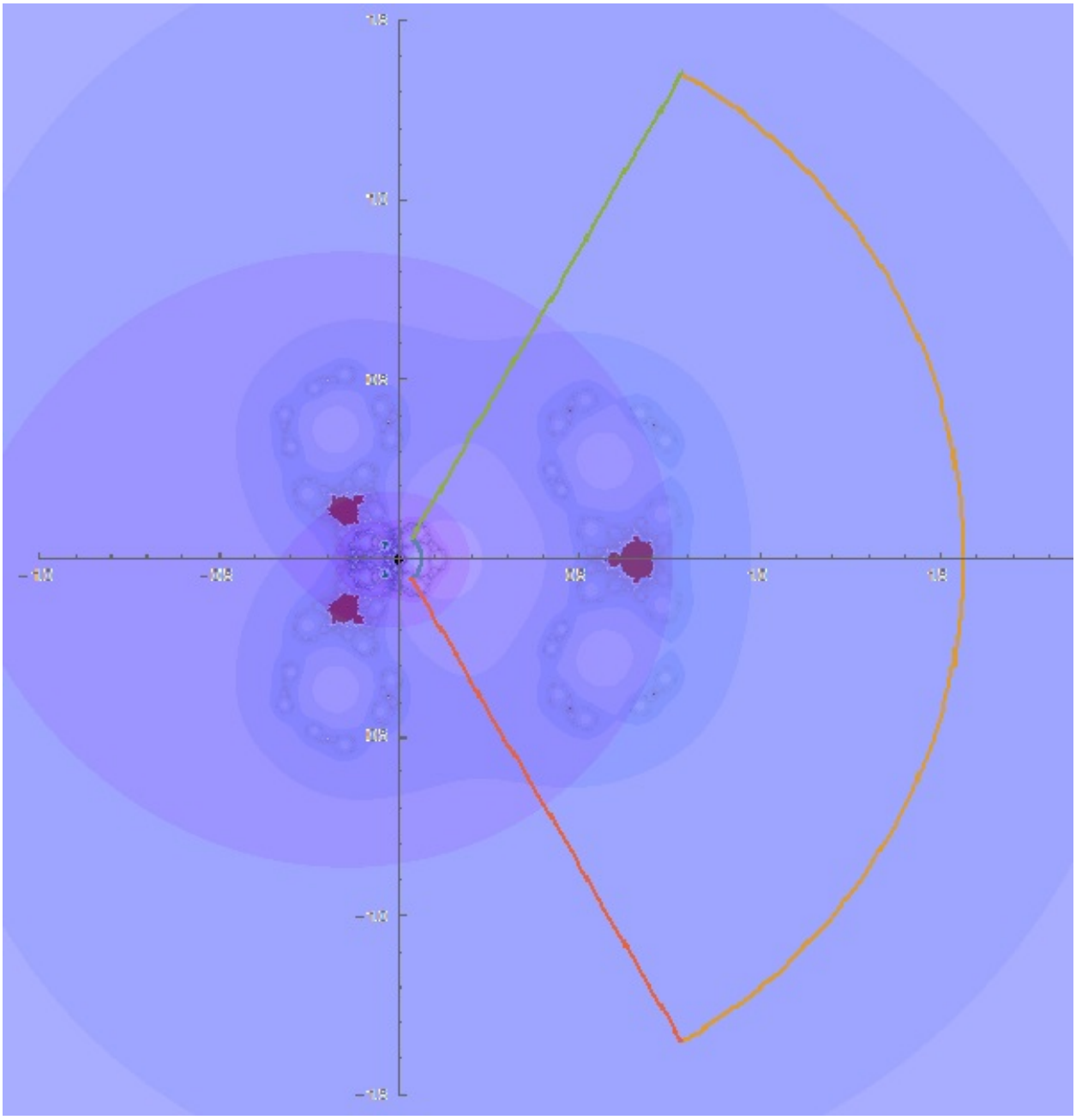

Figure 3.2: A baby $\mathcal{M}$ sitting in $\mathbf{W}_{n,c}$ in the $a$-parameter plane of $R_{n,a,c}$ for $n = 4$ and $c = -0.5$.

With the existence of this baby $\mathcal{M}$ in the $a$-parameter plane, we can use some of the earlier symmetries to prove that another baby $\mathcal{M}$ exists.

**Lemma 3.4.** *For $n$ odd, $R^k_{n,a,-c}(v_-) = -R^k_{n,a,c}(v_+)$, that is that the behavior of the critical orbits are symmetric through $c$ and $-c$.*

*Proof.* Using Lemma 2.2 we find for every positive integer $k$,

$$R^k_{n,a,-c}(v_-) = R^k_{n,a,-c}(-c - 2\sqrt{a}) = R^k_{n,a,-c}(-(c + 2\sqrt{a})) = -R^k_{n,a,c}(c + 2\sqrt{a}) = -R^k_{n,a,c}(v_+)$$

and the critical orbits are symmetric about $c$ and $-c$. □

This result says that $\mathbb{M}^+_{n,c}$ for $c$ is the same as $\mathbb{M}^-_{n,c}$ for $-c$ when $n$ is odd. With this we can combine our results to gain existence of another baby $\mathcal{M}$.

**Corollary 3.5.** *For odd $n \geq 3$ and $0 \leq c \leq 1$, there exists a baby $\mathcal{M}$ associated with $v_-$ in the $a$-parameter plane of $R_{n,a,c}$.*

*Proof.* The proof of this comes from the existence of the $v_+$ baby $\mathcal{M}$ in Theorem 3.3 and the symmetry of the critical orbits in Lemma 3.4. □

Figure 3.3 gives an example $a$-plane of $R_{n,a,c}$ showing the existence of this $v_-$ baby $\mathcal{M}$ in the same spot that a $v_+$ baby $\mathcal{M}$ would be thanks to the symmetry.

## 3.2 Case: $a$ Fixed and Real

We now swap our assumptions and fix $a \in \mathbb{R}$ while allowing $c$ to vary. Now we observe the changes to the critical orbits of $R_{n,a,c}$ in the $c$-parameter plane and find that this can be approached in much the same way as the $a$-parameter case. Our method of drawing the $c$-parameter plane is the same as the $a$-parameter plane. Figure 3.4 shows one example of the $c$-parameter plane of $R_{3,1,c}$. We shall prove the existence of more than one baby $\mathcal{M}$ in this section.

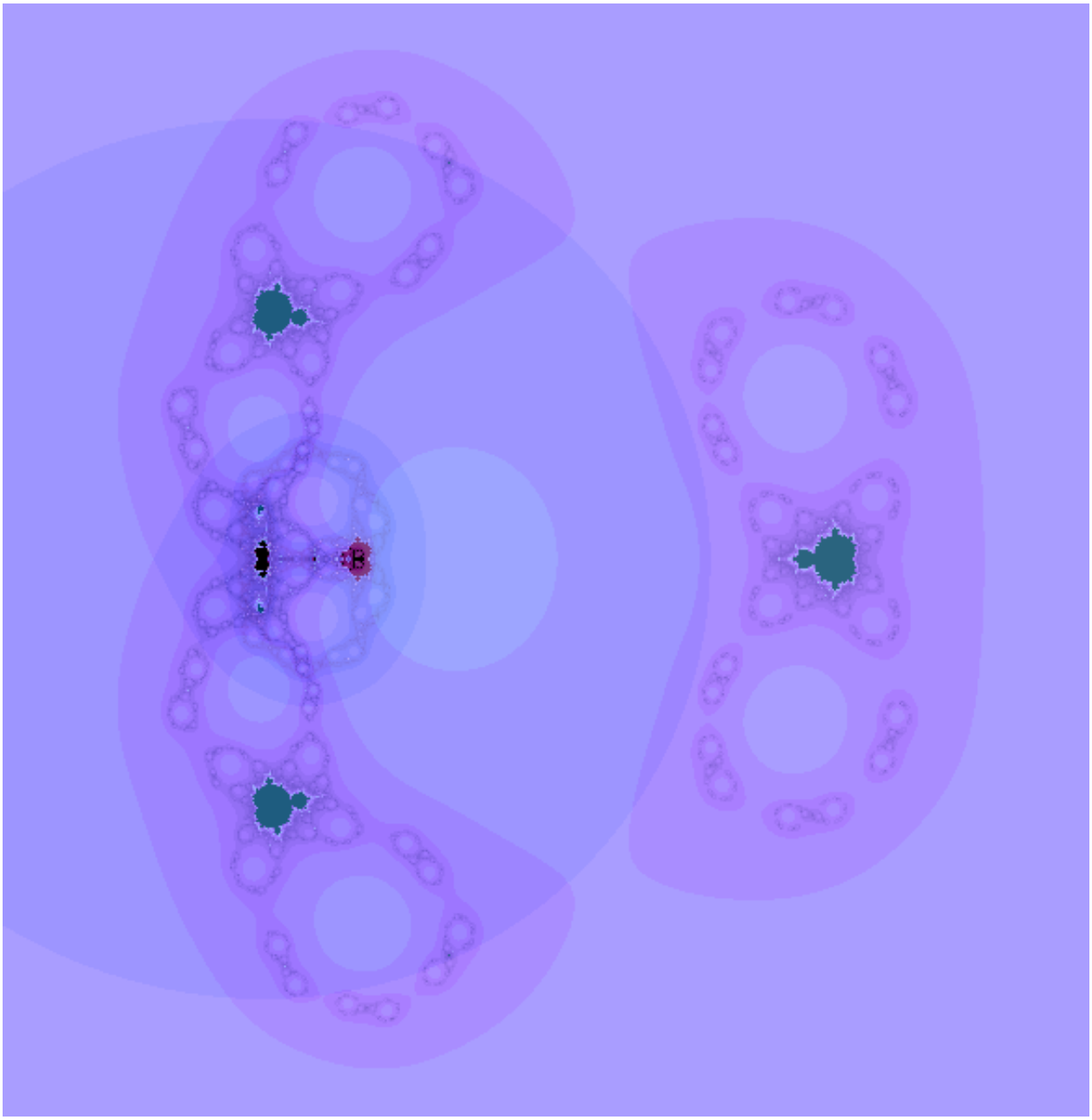

Figure 3.3: The $a$-parameter plane of $R_{n,a,c}$ with $n = 5$ and $c = 0.5$ showing a baby $\mathcal{M}$ associated with $v_-$.

### 3.2.1 First Baby $\mathcal{M}$

Again we follow the same method as before and define a set of $c$ values,

$$\boxed{\mathbf{W}_{n,a} = \left\{ c \;\middle|\; \frac{a^{1/n}}{2} \leq |v_+| \leq 2 \;\; and \;\; \frac{-\pi}{2n} \leq Arg(v_+) \leq \frac{\pi}{2n} \right\}}. \tag{3.2}$$

**Theorem 3.6.** *For $n \geq 3$ and $1 \leq a \leq \dfrac{(2^{n+1}-8)^2}{16}$ the set of $c \in \mathbf{W}_{n,a}$ such that the critical orbit of $v_+$ does not escape $\mathbf{U}'$ is homeomorphic to $\mathcal{M}$.*

*Proof.* It is clear from the definition of $\mathbf{W}_{n,a}$ that $v_+$ will take a closed loop around $\partial\mathbf{U}'$ as $c$ goes around $\partial\mathbf{W}_{n,a}$. $R_{n,a,c}$ is polynomial-like of degree two by Proposition 2.16. We've again satisfied all the criteria needed in Theorem 1.4 and therefore a baby $\mathcal{M}$ exists within $\mathbf{W}_{n,a}$ in the $c$-parameter plane. □

Figure 3.4 gives an example $\mathbf{W}_{n,a}$ where a baby $\mathcal{M}$ associated with $v_+$ lies in a $c$-parameter plane.

### 3.2.2 Multiple Baby $\mathcal{M}$'s in the $c$-plane

From Figure 3.4 we can see there is more than just one baby $\mathcal{M}$ in the $c$-parameter plane. We now prove the existence of some extra baby $\mathcal{M}$'s by mimicking the proof of the existence of the first, then use symmetries to find the rest. For each of these $\mathcal{M}$'s we define a different $\mathbf{U}'$ in the annulus $\mathbf{A}\left(\frac{a^{1/n}}{2}, 2\right)$:

$$\mathbf{U}'_k = \mathbf{U}'_{n,k,a} = \left\{ z = re^{i\theta} \;\middle|\; \frac{|a|^{\frac{1}{n}}}{2} < \; r \; < 2 \;\; and \;\; \frac{4\pi k - \pi}{2n} < \; \theta \; < \frac{4\pi k + \pi}{2n} \right\}$$

for $k = 0, ..., n-1$. Note that $\mathbf{U}'_0 = \mathbf{U}'$.

The image of the outside and inside curves of each $\mathbf{U}'_k$ will still map to the same curve in $U$ as before by Proposition 2.1, so we examine the image of the rays of $\mathbf{U}'_k$.

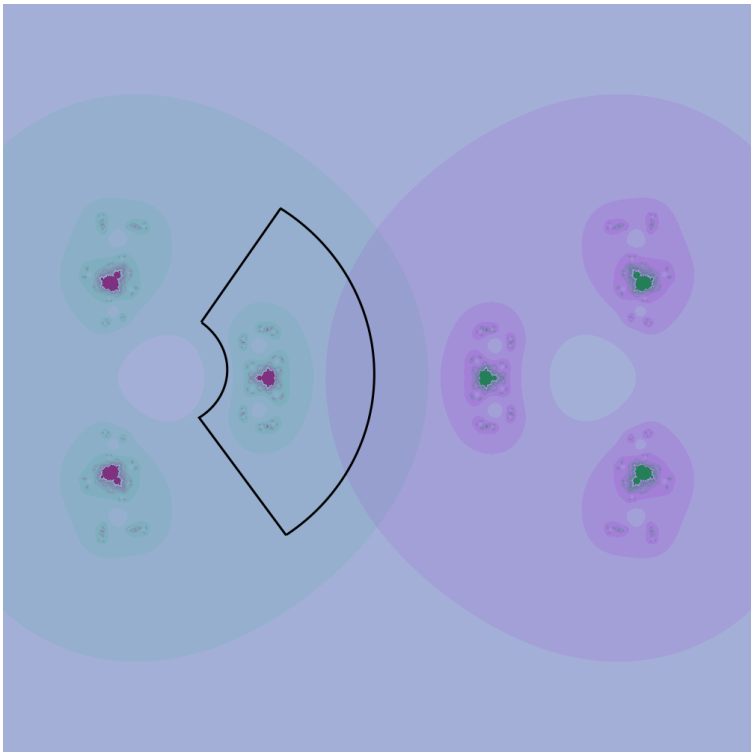

Figure 3.4: The $c$-plane of $R_{n,a,c}$ with $\mathbf{W}_{n,a}$ for $n = 3$ and $a = 1$. Here the center is the origin.

$$\begin{aligned}
R_{n,c,a}\left(r * \exp\left(i\frac{4\pi k \pm \pi}{2n}\right)\right) &= \left(r * \exp\left(i\frac{4\pi k \pm \pi}{2n}\right)\right)^n + \frac{a}{\left(r * \exp\left(i\frac{4\pi k \pm \pi}{2n}\right)\right)^n} + c \\
&= r^n * \exp\left(i\frac{4\pi k \pm \pi}{2}\right) + \frac{a}{r^n * \exp\left(i\frac{4\pi k \pm \pi}{2}\right)} + c \\
&= r^n * \exp\left(i\frac{4\pi k \pm \pi}{2}\right) + \frac{a}{r^n} * \exp\left(i\frac{4\pi k \mp \pi}{2}\right) + c \\
&= \exp\left(i2\pi k\right)\left(r^n * \exp\left(\pm i\frac{\pi}{2}\right) + \frac{a}{r^n} * \exp\left(\mp i\frac{\pi}{2}\right)\right) + c \\
&= \pm\left(r^n - \frac{a}{r^n}\right)i + c.
\end{aligned}$$

We see that $R_{n,a,c}(\mathbf{U}'_k) = R_{n,a,c}(\mathbf{U}')$ for all $k = 0, ..., n-1$ when $\psi = 0$. Now we continue the process by showing that $R_{n,a,c}$ is polynomial-like of degree two on each $\mathbf{U}'_k$.

**Lemma 3.7.** *For $n \geq 3$, $1 \leq a \leq \dfrac{(2^{n+1}-8)^2}{16}$ and $c$ chosen such that $|v_+| \leq 2$, we have $\mathbf{U}'_k \subset \mathbf{U}$ for all $k = 0, 1, ..., n-1$.*

*Proof.* By the proof of Lemma 2.14, $\mathbf{U}'_k \subset \mathbf{D}(0,2) \subset \mathcal{E}$, so we just need to show that for any $k$ the minor axis of $\mathcal{E}$ just intersects $\partial\mathbf{U}'_k$ at worst.

**CASE 1: $\mathbf{U}'_k$ lies in the right half plane:**

As in the proof of Lemma 2.15, the position of the minor axis is $Re(c) = 2 - 2\sqrt{a} \leq 0$ since $a \geq 1$. Thus the minor axis never enters the right-half plane and $\mathbf{U}'_k \subset \mathbf{U}$ for any $\mathbf{U}'_k$ in this case. (See Figure 3.5a)

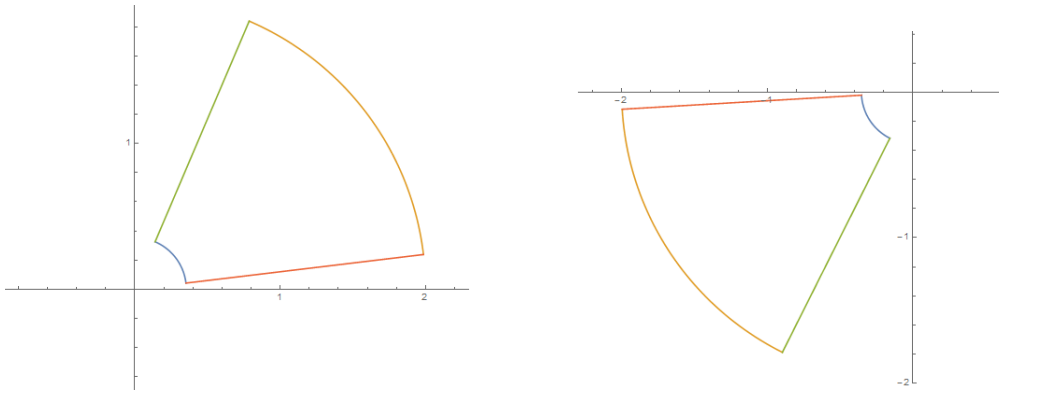

(a) $\mathbf{U}'_k$ in the right half-plane (b) $\mathbf{U}'_k$ in the left half-plane

Figure 3.5: Cases 1 and 2 of Lemma 3.7

**CASE 2: $\mathbf{U}'_k$ lies in the left half plane:**

Now $\mathbf{U}'_k$ lies between the real values of $-2$ and 0. Thus at its greatest,

$$Re(v_+) = 0 \Rightarrow Re(c) = -2\sqrt{a} \leq -2$$

since $a \geq 1$. Here the position of the minor axis will go no farther right than $R(c) = -2$ and the minor axis only touches $\partial\mathbf{U}'_k$ which is admissible since $\mathbf{U}'_k$ is open. Thus $\mathbf{U}'_k \subset \mathbf{U}$ for any $\mathbf{U}'_k$ lying purely in the left-half plane. (See Figure 3.5b)

**CASE 3: $\mathbf{U}'_k$ intersects the imaginary axis:**

The angular width of $\mathbf{U}'_k$ is

$$\frac{4\pi k + \pi}{2n} - \frac{4\pi k - \pi}{2n} = \frac{\pi}{n} \leq \frac{\pi}{3}$$

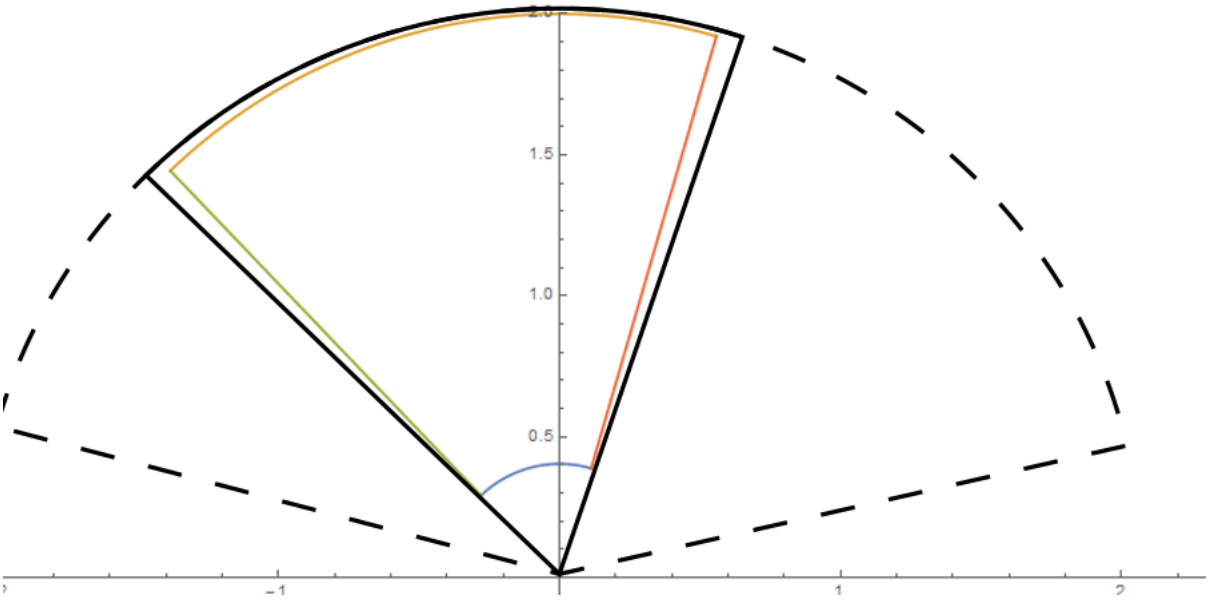


Figure 3.6: $\mathbf{S}_t$ containing a $\mathbf{U}'_k$ that intersects the imaginary axis.

since $n \geq 3$. Assuming for now $\mathbf{U}'_k$ intersects the positive imaginary axis, we define a set:

$$\mathbf{S}_t = \left\{ z \;\middle|\; |z| \leq 2 \;\; and \;\; \frac{\pi}{6} + t\frac{\pi}{3} \leq Arg(z) \leq \frac{\pi}{2} + t\frac{\pi}{3} \right\} \;\; for \; t \in [0,1].$$

For any $t$, $\mathbf{S}_t$ is a wedge of angular width $\frac{\pi}{3}$ that intersects the imaginary axis so any $\mathbf{U}'_k$ that intersects the imaginary axis must be contained in a $\mathbf{S}_t$ for some $t \in [0,1]$. Figure 3.6 gives a sketch of $\mathbf{S}_t$ and the dotted line represents the range of $\mathbf{S}_t$.

In determining the **real-diameter** of $\mathbf{S}_t$, we calculate the distance between the left-most and right-most points of $\mathbf{S}_t$. The left-most point lies on the ray of argument $\frac{\pi}{2} + t\frac{\pi}{3}$ while the right-most point lies on the ray of argument $\frac{\pi}{6} + t\frac{\pi}{3}$. The real values of these points are $r_1 \cos\left(\frac{\pi}{2} + t\frac{\pi}{3}\right)$ and $r_2 \cos\left(\frac{\pi}{6} + t\frac{\pi}{3}\right)$ respectively with $0 \leq r_1, r_2 \leq 2$. Note for this range on $t$, $-1 \leq \cos\left(\frac{\pi}{2} + t\frac{\pi}{3}\right) \leq 0$ and $0 \leq \cos\left(\frac{\pi}{6} + t\frac{\pi}{3}\right) \leq 1$. This means that the endpoints of these rays, at $r_1 = r_2 = 2$, will be the farthest left and right points of $\mathbf{S}_t$. The real-diameter is the difference of these two values,

$$2\cos\left(\frac{\pi}{6} + t\frac{\pi}{3}\right) - 2\cos\left(\frac{\pi}{2} + t\frac{\pi}{3}\right) \tag{3.3}$$

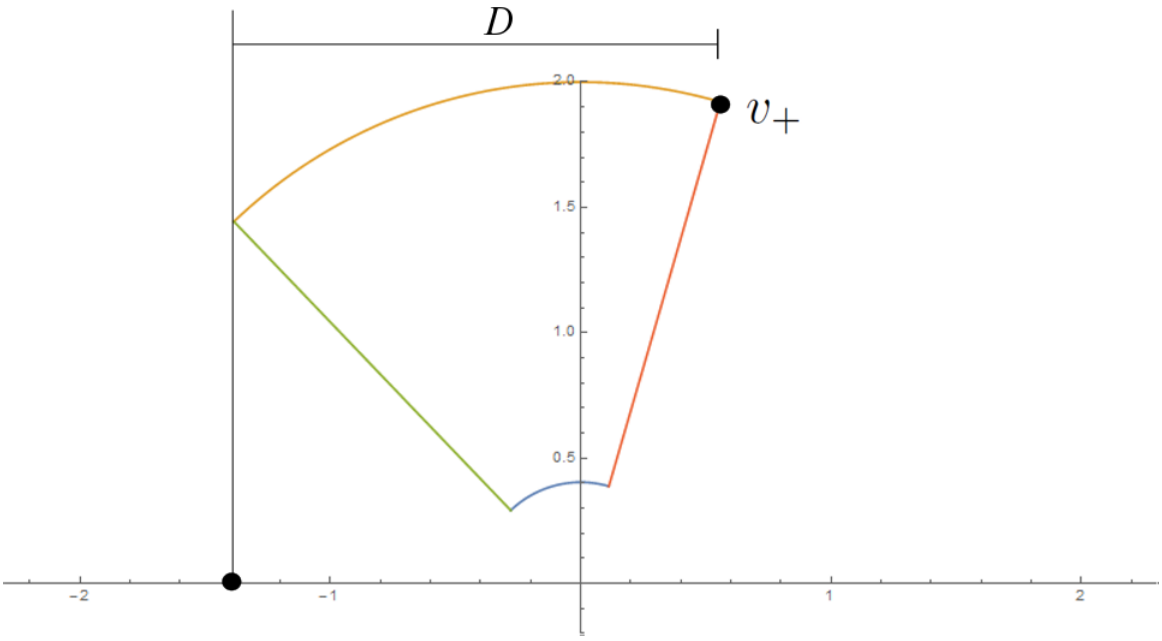


Figure 3.7: A $\mathbf{U}'_k$ intersecting the imaginary axis. The maximum width of $\mathbf{U}'$ is $D = 2\sqrt{a} \geq 2$ from $v_+$ to the minor axis of $\mathcal{E}$. The vertical line, $x = Re(c)$, is the minor axis of $\mathcal{E}$.

Using differentiation to find the maximum on equation (3.3), we find the max value of the width occurs at $t = \frac{1}{2}$. Plugging this in, we find the width to be 2, thus $\mathbf{S}_t$ is no wider than 2 units. This means the "real-width" of $\mathbf{U}'_k$ is at most 2 (since $\mathbf{U}'_k \subset \mathbf{S}_t$). We also find the real-diameter between $v_+$ and the minor axis of $\mathcal{E}$, remembering that $Re(c)$ is the position of the minor axis of $\mathcal{E}$

$$Re\left(c + 2\sqrt{a}\right) - Re(c) = Re(c) + 2\sqrt{a} - Re(c) = 2\sqrt{a} \geq 2$$

since $a \geq 1$. Therefore when $v_+$ is at the right-most point of $\mathbf{U}'_k$, the minor axis will be a distance of at least 2 units to the left, a distance greater than or equal to the "real-width" of $\mathbf{U}'_k$. (See Figure 3.7)

A symmetrical argument can be used for any $\mathbf{U}'_k$ that intersects the negative imaginary axis and thus $\mathbf{U}'_k \subset \mathbf{U}$ for all $k = 0, 1, ..., n-1$.

□

With $\mathbf{U}'_k \subset \mathbf{U}$ for all $k = 0, 1, ..., n-1$, we have the prerequisites for a polynomial-like map.

**Proposition 3.8.** *With the same hypotheses as the previous lemma, $R_{n,a,c}$ is a polynomial like map of degree two on $\mathbf{U}'_k$ for any $k = 0, 1, ..., n-1$.*

*Proof.* By design, each $\mathbf{U}'_k$ is centered around a unique critical point of $R_{n,a,c}$, $|a|^{\frac{1}{2n}} e^{i\frac{2\pi k}{n}}$. $R_{n,a,c}$ is also a two-to-one map on each $\mathbf{U}'_k$ by discussion above. With this, the previous lemma, and the fact that $R_{n,a,c}$ is analytic on each $\mathbf{U}'_k$, $R_{n,a,c}$ is a polynomial-like map of degree two on each $\mathbf{U}'_k$. □

Now we can define a $\mathbf{W}$ associated with each new $\mathbf{U}'_k$,

$$\boxed{\mathbf{W}_{n,a,k} = \left\{ c \;\middle|\; \frac{a^{1/n}}{2} \leq \left|c + 2\sqrt{a}\right| \leq 2 \;\; and \;\; \frac{4\pi k - \pi}{2n} \leq Arg(c + 2\sqrt{a}) \leq \frac{4\pi k + \pi}{2n} \right\}} \quad (3.4)$$

which leads into our next theorem.

**Theorem 3.9.** *Given $n \geq 3$, $1 \leq a \leq \dfrac{(2^{n+1}-8)^2}{16}$, and a fixed $k \in \{0, 1, ..., n-1\}$, the set of $c \in \mathbf{W}_{n,a,k}$ such that the critical orbit of $v_+$ does not escape $\mathbf{U}'_k$ is homeomorphic to $\mathcal{M}$.*

*Proof.* By design, as $c$ makes a closed loop around $\partial\mathbf{W}_{n,a,k}$, then $v_+$ will make a closed loop around $\partial\mathbf{U}'_k$ and all the criterion of Theorem 1.4 and Proposition 3.8 are satisfied. □

See Figure 3.8 for an example.

### 3.2.3 Baby $\mathcal{M}$'s associated with $v_-$

Theorem 3.9 proves that $n$ distinct baby $\mathcal{M}$'s associated with $v+$ exist in the $c$-plane, but we can see from Figure 3.4 that there are other baby $\mathcal{M}$'s associated with the other critical orbit, $v_-$. Next we show symmetries among the critical orbits that allow for us to prove quickly the existence of more baby $\mathcal{M}$'s.

First we note that Lemma 3.4 shows that $\mathbb{M}_{n,a}$ is symmetric through the origin of the $c$-plane. We will combine this result with the following symmetries.

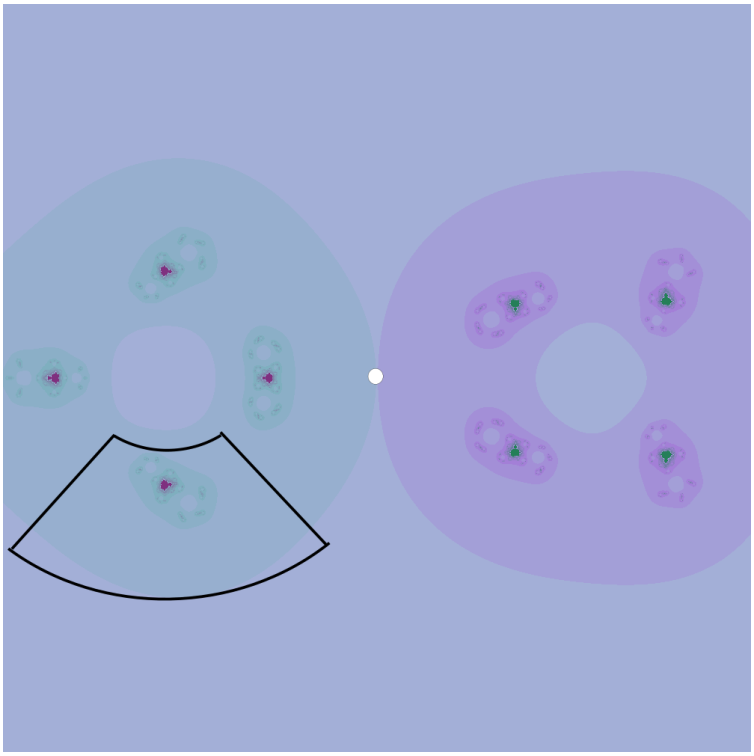

Figure 3.8: The $c$-parameter plane of $R_{n,a,c}$ and $\mathbf{W}_{n,a,k}$ with $n = 4$, $a = 1$, and $k = 3$. The white dot is the origin.

**Lemma 3.10.** *For $n \geq 3$ and $a$ real, the critical orbits of $R_{n,a,c}$ are symmetric about $c$ and $\bar{c}$. In other words, the critical orbits of $R_{n,a,c}$ are symmetric over the real axis in the $c$-plane.*

*Proof.* Using Lemma 2.4 and the fact that $a$ is real, we find:

$$\overline{R^k_{n,a,\bar{c}}(v_\pm)} = \overline{R^k_{n,a,\bar{c}}(\bar{c} \pm 2\sqrt{a})} = \overline{R^k_{n,a,\bar{c}}(\overline{c \pm 2\sqrt{a}})} = R^k_{n,a,c}(c \pm 2\sqrt{a}) = R^k_{n,a,c}(v_\pm).$$

This equation yields that the dynamics of the critical orbits above the real axis of the $c$-plane will be the same as the dynamics below. Therefore $\mathbb{M}_{n,a}$ is symmetric with respect to the real axis. □

So Lemmas 3.4 and 3.10 show that $\mathbb{M}_{n,a}$ is symmetric through the origin and over the real-axis respectively in the $c$-plane for $n$ odd and $a$ real. A third symmetry can be derived from the composition of these two.

**Lemma 3.11.** *For $n \geq 3$, odd, and $a$ real, $\mathbb{M}_{n,a}$ is symmetric over the imaginary axis in the $c$-plane.*

With these symmetries established and the existence of $n$ baby $\mathcal{M}$'s from Theorem 3.9, we get the existence of more baby $\mathcal{M}$'s in the $c$-plane.

**Theorem 3.12.** *If $n \geq 3$, odd, and $1 \leq a \leq \frac{(2^{n+1}-8)^2}{16}$, then for each baby $\mathcal{M}$ associated with the critical orbit of $v_+$, there exists a matching baby $\mathcal{M}$ associated with the critical orbit of $v_-$. Each $v_-$ baby $\mathcal{M}$ is a reflection of a $v_+$ baby $\mathcal{M}$ over the imaginary axis of the $c$-plane.*

*Proof.* This is a result of Theorem 3.9 and Lemma 3.11 and thus there are $2n$ baby $\mathcal{M}$'s in the $c$-plane under these restrictions of $n$ and $a$. □

Figure 3.9 gives an example of the $c$-plane with $2n$ baby $\mathcal{M}$'s.

### 3.2.4 Existence of Baby $\mathcal{M}$'s for smaller $a$-values

Having established the existence of $2n$ baby $\mathcal{M}$'s, we now look to expand the range in which they exist. We shall prove the existence of baby $\mathcal{M}$'s in the $c$-plane for smaller values of $a$, as small as $\frac{1}{10}$.

Smaller values of $a$ force us to condense our escape radius of $R_{n,a,c}$ as well as put more of a restriction on the degree of the rational functions. We shall prove for $\frac{1}{10} \leq |a| \leq 1$ that any point outside of a modulus of 1.25 will escape to $\infty$ under $R_{n,a,c}$ (instead of 2 before).

Given this escape radius and $a$ at its max, having $|c| \geq 3.25$ will guarantee that $v_+ \in A^*(\infty)$ (i.e. $v_+$ lies outside the escape radius).

**Lemma 3.13.** *If $n \geq 11$, $|c| \leq 3.25$, $\frac{1}{10} \leq a \leq 1$, then any $z$ such that $|z| > \frac{5}{4}$ will lie in $A^*(\infty)$ of $R_{n,a,c}$.*

*Proof.* Once again using the results by Boyd and Schulz in [HS11], given any $\epsilon > 0$ and for $n$ sufficiently large, the filled Julia set of $R_{n,a,c}$ is contained in $\mathbf{D}_{1+\epsilon}$. Anything outside the radius of $1 + \epsilon$ escapes to $\infty$.

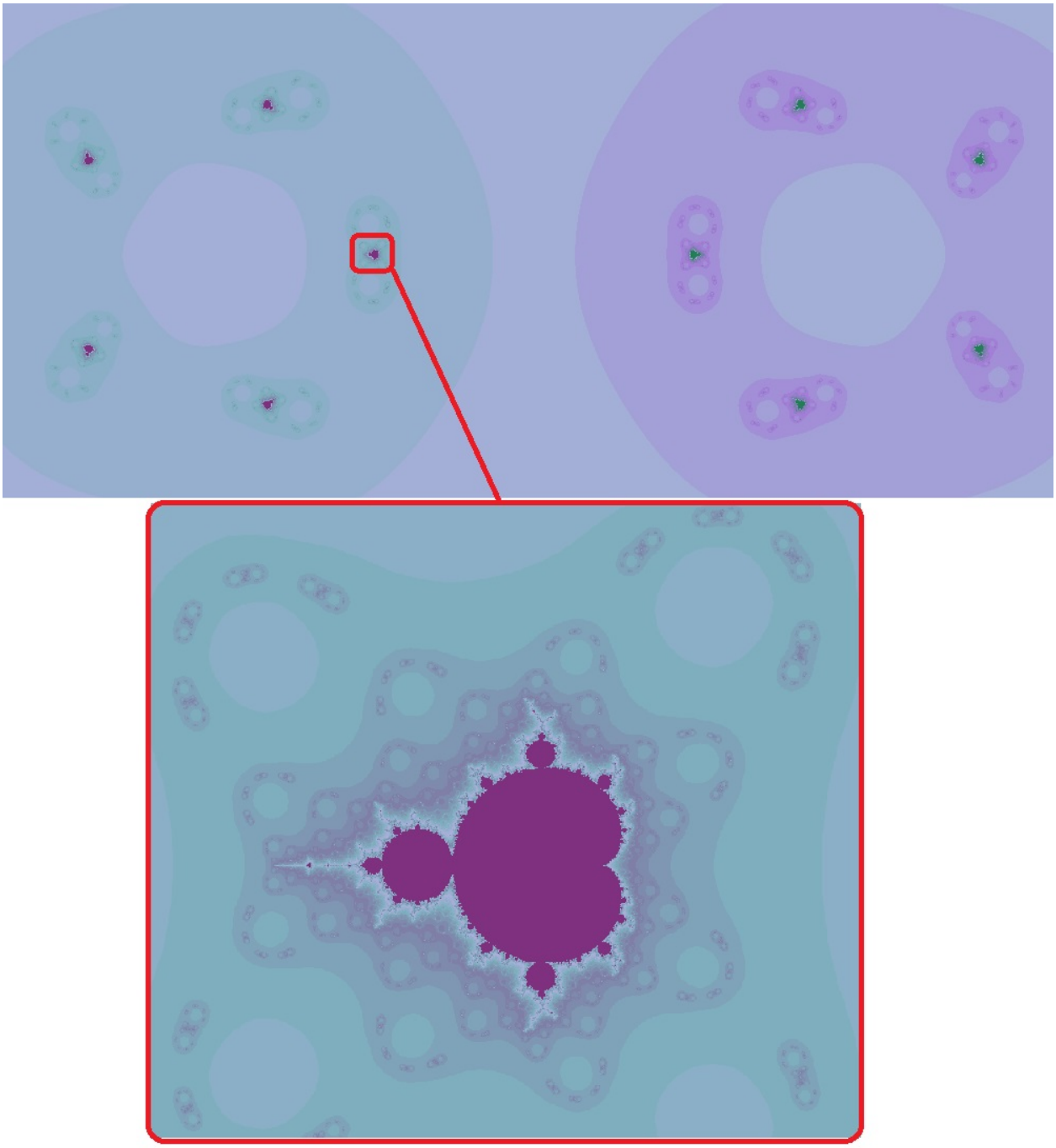

Figure 3.9: The $c$-parameter plane of $R_{n,a,c}$ showing 10 baby $\mathcal{M}$'s for $n = 5$ and $a = 1$.

Similar to Lemma 2.6, if $N$ satisfies $(1+\epsilon)^N > 3Max\{1, |a|, |c|\}$, then for $n \geq N$ the orbits of values $|z| > 1+\epsilon$ must tend to $\infty$. For us $\epsilon = 0.25$, and $3Max\{1, |a|, |c|\} = 9.75$ for $a$ and $c$ at their greatest moduli. So when we solve this equation for $N$, we find $N > \dfrac{ln(9.75)}{ln(1.25)} \approx 10.2$, thus $n \geq 11$ will satisfy the criterion. □

Combining this new escape criterion with Lemma 2.1 yields that the orbit of any $|z| < \dfrac{4}{5}a^{\frac{1}{n}}$ will tend to $\infty$, thus we get the following lemma.

**Lemma 3.14.** *Under the same hypothesis as Lemma 3.13, the filled Julia set of $R_{n,a,c}$ is contained in the annulus* $\mathbf{A}\left(\dfrac{4}{5}a^{\frac{1}{n}}, \dfrac{5}{4}\right)$.

With this new restriction on the location of the filled Julia set of $R_{n,a,c}$, we define a set $\mathcal{U}'$ that takes on the same role as that of $\mathbf{U}'$ from earlier. We prove $R_{n,a,c}$ is polynomial-like of degree two on this set:

$$\boxed{\mathcal{U}' = \left\{ z = re^{i\theta} \;\middle|\; \frac{4}{5}a^{\frac{1}{n}} < \; r \; < \frac{5}{4} \;\; and \;\; \frac{\psi - \pi}{2n} < \; \theta \; < \frac{\psi + \pi}{2n} \right\}} \tag{3.5}$$

where $\psi = Arg(a) = 0$ since $a \in \mathbb{R}^+$. We also define $\mathcal{U} = R_{n,a,c}(\mathcal{U}')$. The critical point $a^{\frac{1}{2n}}$ is contained in this new $\mathcal{U}'$ and is mapped to $v_+$. With this change to the inner and outer boundaries of $\mathcal{U}'$, the image under $R_{n,a,c}$ is still half an ellipse cut by the minor axis and centered at $c$ but now has

$$\text{semi-major axis length : } \quad \left(\frac{5}{4}\right)^n + \left(\frac{4}{5}\right)^n |a|$$

$$\text{semi-minor axis length : } \quad \left(\frac{5}{4}\right)^n - \left(\frac{4}{5}\right)^n |a|$$

We refer to this new ellipse as $\mathcal{L}$. Similar to above, we must show that $R_{n,a,c}$ is polynomial-like of degree two on $\mathcal{U}'$. First we will show $\mathcal{U}'$ is contained in $\mathcal{L}$ described above and then show further containment of $\mathcal{U}'$ inside $\mathcal{U}$.

**Lemma 3.15.** $\mathcal{U}' \subset \mathcal{L}$ *for* $n \geq 11$, $\dfrac{1}{10} \leq a \leq 1$, *and* $c$ *such that* $|v_+| \leq \dfrac{5}{4}$.

*Proof.* Similar to the proofs of Lemmas 2.10 and 2.14, we shall define the ellipse by its alternate definition:

$$\left\{ z \;\middle|\; |z-(c-\sqrt{a})|+|z-(c+\sqrt{a})| \leq 2\left(\left(\frac{5}{4}\right)^n+\left(\frac{4}{5}\right)^n|a|\right)\right\}. \tag{3.6}$$

Since $\mathcal{U}' \subset \mathbf{D}(0,\frac{5}{4})$, then proving $\mathbf{D}(0,\frac{5}{4})$ is contained in the ellipse is satisfactory. The largest values of $|v_\pm|$ will be observed. We start with $|v_+| = \frac{5}{4}$ on the outer boundary and find the largest possible $|v_-|$:

$$\begin{aligned} |v_+| &= |c+2\sqrt{a}| = \frac{5}{4} \;\Rightarrow\; c = \frac{5}{4}e^{i\theta} - 2\sqrt{a} \\ &\Rightarrow \quad |v_-| = |c-2\sqrt{a}| = \left|\frac{5}{4}e^{i\theta} - 4\sqrt{a}\right| \end{aligned}$$

for some $\theta \in [0, 2\pi)$. Using derivatives we find the maximum of $|v_-|$ occurs at $\theta = \pi$, so the max $|v_-|$ is $\frac{5}{4} + 4\sqrt{a}$, and we have bounds on the foci.

Now we have:

$$\begin{aligned} & |z-(c-\sqrt{a})|+|z-(c+\sqrt{a})| \\ \leq\ & 2|z| + |c+2\sqrt{a}| + |c-2\sqrt{a}| \\ \leq\ & 2\left(\frac{5}{4}\right) + \left(\frac{5}{4}\right) + \left(\frac{5}{4}+4\sqrt{a}\right) \\ =\ & 5+4\sqrt{a} \\ \leq\ & 5+4 \ (\textit{Since } a \leq 1) \\ \leq\ & 2\left(\frac{5}{4}\right)^{11} \leq\ 2\left(\left(\frac{5}{4}\right)^n+\left(\frac{4}{5}\right)^n|a|\right). \end{aligned}$$

Thus the image of any point in $\mathcal{U}' \subset \mathbf{D}(0,\frac{5}{4})$ will be contained in this ellipse.

□

With $\mathcal{U}'$ contained in the ellipse, we just need to show the minor axis of the ellipse does not intersect $\mathcal{U}'$. This will guarantee that $\mathcal{U}' \subset \mathcal{U}$.

**Lemma 3.16.** *For $n \geq 11$, $\frac{1}{10} \leq a \leq 1$, and $c$ such that $|v_+| \leq \frac{5}{4}$, $\mathcal{U}' \subset \mathcal{U}$.*

*Proof.* $\mathcal{U}$ is the half of the ellipse that contains $v_+$ which is the right-half in this case. We just have to show the minor axis of the ellipse does not intersect $\mathcal{U}'$ and in fact lies to the left to $\mathcal{U}'$.

The minor axis is a straight vertical line centered at $c$. Its horizontal position is $Re(c)$, a value that depends on $v_+$. At its greatest modulus we observe $v_+$ on the outer arc of $\mathcal{U}'$, so $c + 2\sqrt{a} = \frac{5}{4}e^{i\theta}$ for $|\theta| \leq \frac{\pi}{2n}$, thus

$$Re(c) = \frac{5}{4}\cos(\theta) - 2\sqrt{a} \ \leq \ \frac{5}{4} - 2\sqrt{a}.$$

Now we show the minor axis lies to the left of the inner arc of $\mathcal{U}'$. This happens if

$$Re(c) < Re\left(\frac{4}{5}a^{\frac{1}{n}}e^{i\theta}\right), \ i.e. \ \frac{5}{4} - 2\sqrt{a} < \frac{4}{5}a^{\frac{1}{n}}\cos(\theta).$$

Since $n \geq 11$, $\cos(\theta)$ will be minimal at $\theta = \pm\frac{\pi}{2n}$ and thus the minimum value of $Re\left(\frac{4}{5}a^{\frac{1}{n}}e^{i\theta}\right)$ will be $\frac{4}{5}a^{\frac{1}{n}}\cos\left(\frac{\pi}{2n}\right)$ with respect to $\theta$. To minimize further we take a derivative with respect to $n$ and find

$$\frac{\partial}{\partial_n}\left(\frac{4}{5}a^{\frac{1}{n}}\cos\left(\frac{\pi}{2n}\right)\right) = \frac{2a^{1/n}\left(\pi\sin\left(\frac{\pi}{2n}\right) - 2\cos\left(\frac{\pi}{2n}\right)ln(a)\right)}{5n^2} > 0$$

since $a \leq 1$. Therefore the derivative is positive and the horizontal position of the inner arc of $\mathcal{U}'$ increases as n increases. As $\frac{4}{5}a^{\frac{1}{n}}\cos\left(\frac{\pi}{2n}\right)$ increases with $a$ as well, then the minimum value of this equation occurs at the minimal values of $n = 11$ and $a = \frac{1}{10}$. Thus

$$Re\left(\frac{4}{5}a^{\frac{1}{n}}e^{i\theta}\right) \geq \frac{4}{5}(0.1)^{\frac{1}{11}}\cos\left(\frac{\pi}{22}\right) \approx 0.6423.$$

At this point the minor axis will be located at $\frac{5}{4} - 2\sqrt{0.1} \approx 0.618$, and we have that the minor axis lies to the left of $\mathcal{U}'$. The horizontal position of the minor axis does not depend on $n$ and moves to the left as $a$ increases. With this it is assured that the minor axis of the ellipse will never pass through $\mathcal{U}'$ and $\mathcal{U}' \subset \mathcal{U}$. □

**Proposition 3.17.** *With the same assumptions as Lemma 3.16, $R_{n,a,c} : \mathcal{U}' \to \mathcal{U}$ is a polynomial-like map of degree two.*

*Proof.* $R_{n,a,c}$ is analytic on $\mathcal{U}'$ by choice of the boundaries as well as two-to-one with a single critical point. With this, $R_{n,a,c}$ satisfies the definition of a polynomial-like map of degree two by Lemma 3.16. □

With a family of degree two polynomial-like maps we now define a $\mathcal{W}_{n,a}$ for this case to invoke Theorem 1.4,

$$\boxed{\mathcal{W}_{n,a} = \left\{ c \;\middle|\; \frac{4}{5}a^{1/n} \leq \left|c + 2\sqrt{a}\right| \leq \frac{5}{4} \;\; and \;\; \frac{-\pi}{2n} \leq Arg(c + 2\sqrt{a}) \leq \frac{\pi}{2n} \right\}} \tag{3.7}$$

and follow the same criterion to show that a baby $\mathcal{M}$ is contained in this $\mathcal{W}_{n,a}$.

**Theorem 3.18.** *For $\frac{1}{10} \leq a \leq 1$ and $n \geq 11$, the set of c-values contained in $\mathcal{W}_{n,a}$ such that the critical orbit of $v_+$ does not escape $\mathcal{U}'$ is homeomorphic to $\mathcal{M}$.*

*Proof.* By design of $\mathcal{W}_{n,a}$ it is clear that as $c$ loops around $\partial\mathcal{W}_{n,a}$, we have $v_+$ will make a loop around $\partial\mathcal{U}' \subset \mathcal{U} - \mathcal{U}'$.

$R_{n,a,c}$ is polynomial-like of degree two on $\mathcal{U}'$ by Proposition 3.17 and we satisfy the criterion of Theorem 1.4. Thus there exists a baby $\mathcal{M}$ in $\mathcal{W}_{n,a}$. □

We have now extended the interval of $a$-values in which a baby $\mathcal{M}$ associated with $v_+$ exists in the $c$-plane, but restricted on the degree of $R_{n,a,c}$. We now get a result for free.

**Corollary 3.19.** *For $\frac{1}{10} \leq a \leq \frac{(2^{n+1} - 8)^2}{16}$ and $n \geq 11$, there exists a baby $\mathcal{M}$ associated with $v_+$ lying in the c-parameter plane of $R_{n,a,c}$.*

*Proof.* This is a result of combining Theorems 3.6 and 3.18 with an intersection on their criterion on $n$. □

Because of the existing symmetries in the $c$-plane we get a baby $\mathcal{M}$ associated with $v_-$ under these criterion on $a$ and $n$ as well.

**Corollary 3.20.** *For $n \geq 11$, odd, and $\frac{1}{10} \leq a \leq \frac{(2^{n+1}-8)^2}{16}$, there exists a baby $\mathcal{M}$ associated with $v_-$ lying in the $c$-parameter plane of $R_{n,a,c}$*

*Proof.* This follows from the existence of a baby $\mathcal{M}$ associated with $v_+$ in Corollary 3.19 as well as the symmetry given in Lemma 3.11. Therefore the baby $\mathcal{M}$ associated with $v_-$ is a reflection of the baby $\mathcal{M}$ associated with $v_+$ from Corollary 3.19 over the imaginary axis of the $c$-parameter plane of $R_{n,a,c}$. □

In Figure 3.10 we can see an example of these baby $\mathcal{M}$'s existing under these new criterion. A zoom in is necessary as the baby $\mathcal{M}$'s seem to get smaller as $n$ increases. The green baby $\mathcal{M}$ represents the orbit of $v_-$ and the purple baby $\mathcal{M}$ represents the orbit of $v_+$.

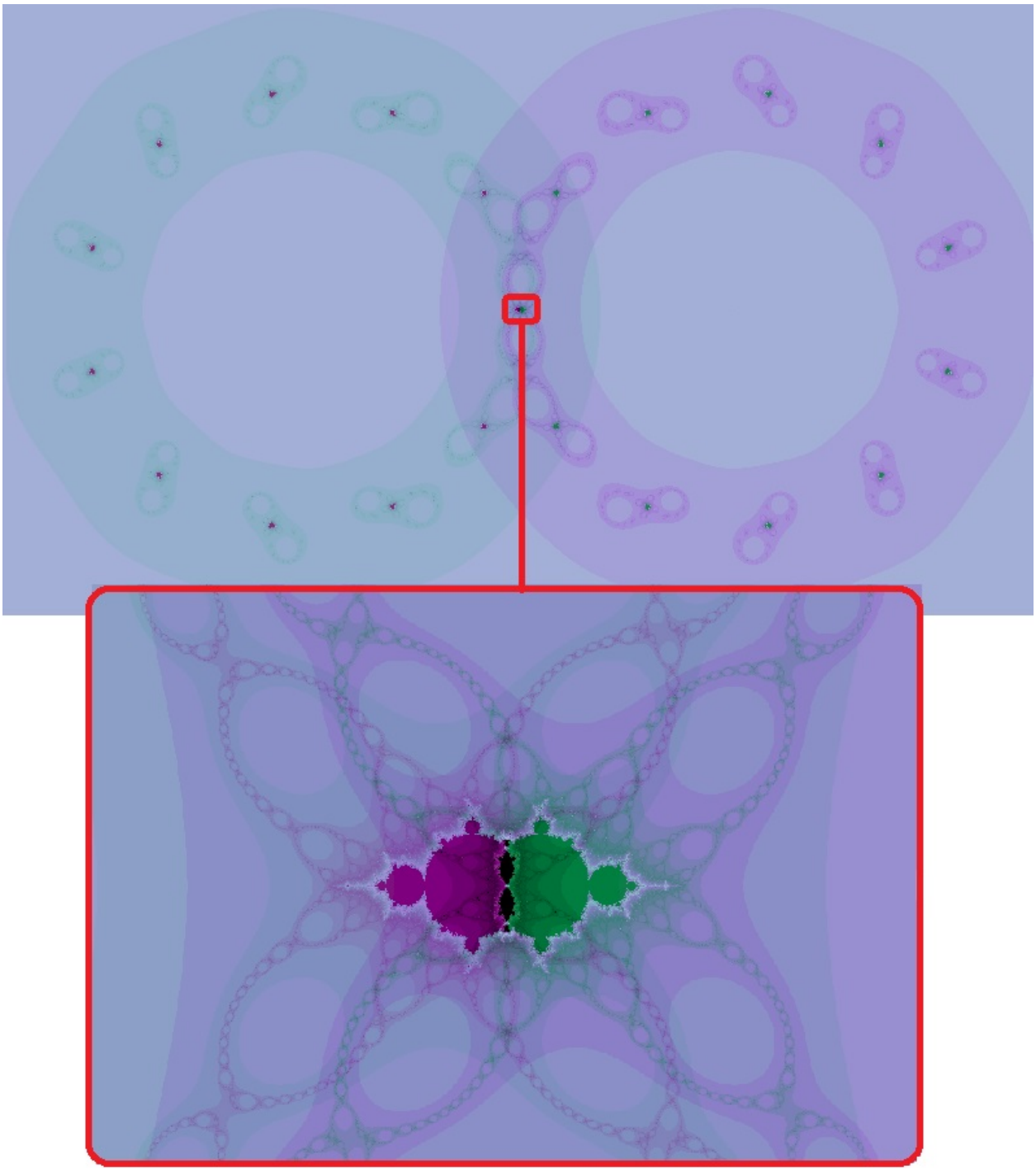

Figure 3.10: The $c$-parameter plane of $R_{n,a,c}$ for $n = 11$ and $a = 0.22$ with a zoom in on the origin. The green $\mathcal{M}$ is associated with $v_-$ and the purple $\mathcal{M}$ is associated with $v_+$.

# Chapter 4

# Next Steps

This section continues work in the $c$-parameter plane of $R_{n,a,c}$ but the same principles can be applied to the $a$-parameter plane. There are interesting occurrences in the boundedness loci surrounding the known baby $\mathcal{M}$'s. The computer pictures of these parameter planes have revealed phenomena that otherwise would not have been noticed.

## 4.1 More copies of $\mathcal{M}$

We have shown the existence of multiple baby $\mathcal{M}$'s for various criteria on $n$, $a$, and $c$, but when observing the pictures, we can see more baby $\mathcal{M}$'s in the $a$-parameter plane than what Theorem 3.3 and Corollary 3.4 suggest. Figure 3.2 for example shows more than just the single established baby $\mathcal{M}$ in the $a$-parameter plane.

Devaney was able to prove the existence of more baby $\mathcal{M}$'s in the $a$-plane using a rotational symmetry of the boundedness locus about the origin the plane [Dev06]. We do not have such a symmetry present, but what can be said is that the baby $\mathcal{M}$'s in the $a$-parameter plane of $R_{n,a,c}$ must distribute into a limaçon for $c \neq 0$ [HS11].

Further observations of the parameter planes suggest there are even more baby $\mathcal{M}$'s at smaller scales in the boundedness loci and Figure 4.1 gives one such example. Both [BCDF15] and [Dev09b] show there are an infinite number of small homeomorphic copies of $\mathcal{M}$ in the

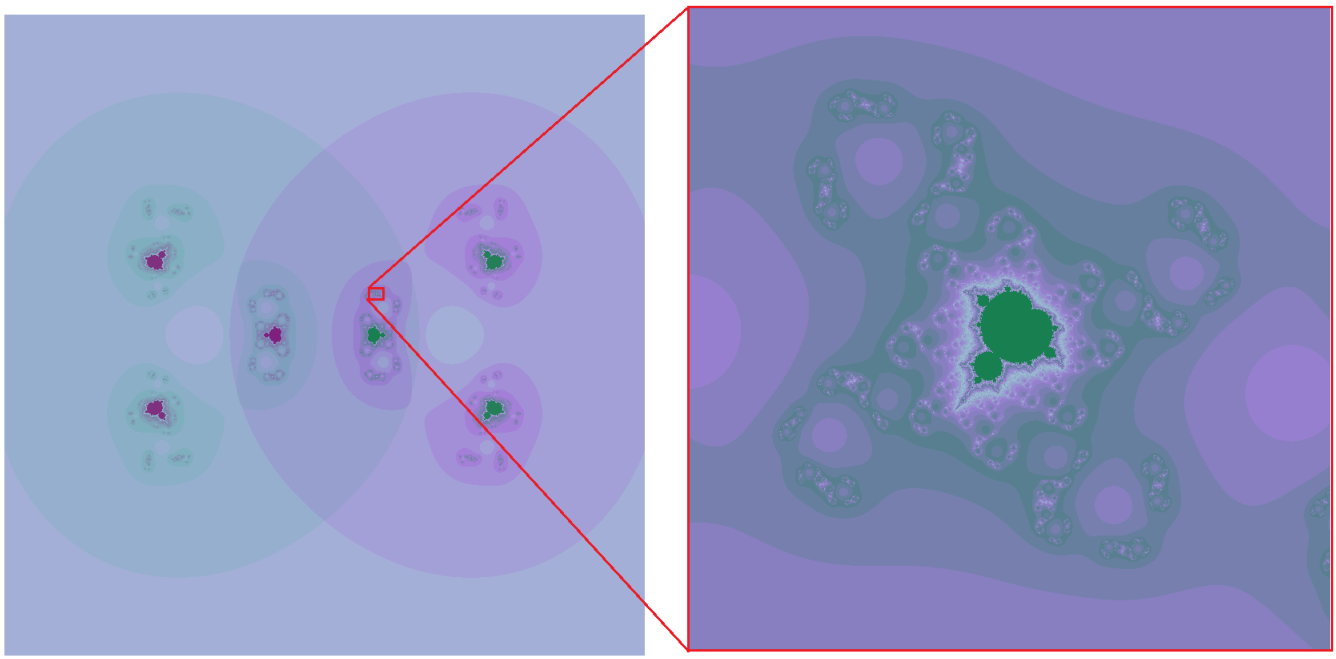

Figure 4.1: A zoom-in on the boundedness locus in the $c$-parameter plane of $R_{n,a,c}$ for $n = 3$ and $a = 0.5$.

$a$-parameter plane of $R_{n,a,0}$. We observe these smaller copies of $\mathcal{M}$ spread throughout the boundedness loci of both the $c$-parameter and $a$-parameter planes of $R_{n,a,c}$.

The techniques used in [BCDF15] take advantage of **external rays** of $\mathcal{M}$. It is known there exists an analytic uniformizing map $\Phi$ that maps in one-to-one fashion the exterior of the unit disk in $\mathbb{C}$ to the exterior of $\mathcal{M}$. The **external ray** of argument $\theta$ is the image of the line $\left\{te^{2\pi i\theta} \mid t > 1\right\}$ under $\Phi$. [BCDF15] shows that some smaller copies of $\mathcal{M}$ lie on certain external rays. In [Dev09b] the rays are extended to the interior of the boundedness locus to show the placement of more small copies of $\mathcal{M}$. These rays become a recurring theme for the family $R_{n,a,0}$ and it seems likely that they have an importance in the case of $c \neq 0$.

## 4.2 Other Interesting Shapes in the Boundedness Loci

With the existence of multiple baby $\mathcal{M}$'s simultaneously, the discussion of their location and movement throughout the parameter planes as parameters vary is another topic of study. In particular, the cases for which two baby $\mathcal{M}$'s overlap opens up more topics of interest.

We first give a precise location of two baby $\mathcal{M}$'s from Corollaries 3.19 and 3.20. With a better understanding of where they are located, we can give a range of $a$-values for which we know the baby $\mathcal{M}$'s intersect.

We define the center of a baby $\mathcal{M}$ in the $c$-parameter plane to be the $c$-value for which the critical point is the same as the critical value. In other words the critical point is a fixed point of $R_{n,a,c}$. If we wish to find the center of a baby $\mathcal{M}$ associated with $v_+$, then we are solving the equation $a^{1/2n} = c + 2\sqrt{a}$ for $c$, which is

$$c_+ = a^{1/2n} - 2\sqrt{a}.$$

By Lemma 3.11, the baby $\mathcal{M}$ associated with $v_-$ is just a reflection over the imaginary axis of the $c$-parameter plane. We reflect $c_+$ over the imaginary axis to find the center of the baby $\mathcal{M}$ associated with $v_-$ to be

$$c_- = 2\sqrt{a} - a^{1/2n}.$$

With this we can give an exact case when the two baby $\mathcal{M}$'s overlap.

**Proposition 4.1.** *For $n \geq 11$, odd, and $a = \left(\frac{1}{4}\right)^{\frac{n}{n-1}}$, two baby $\mathcal{M}$'s in the c-parameter plane associated with $v_+$ and $v_-$ respectively overlap and have the same center. Further, this same center is in fact the origin of the c-plane.*

*Proof.* We first solve the equation

$$c_+ = c_- \Rightarrow a^{1/2n} - 2\sqrt{a} = 2\sqrt{a} - a^{1/2n} \Rightarrow 2\sqrt{a} = a^{1/2n} \Rightarrow a = 2^{\frac{1}{\frac{1}{2n} - \frac{1}{2}}} = \left(\frac{1}{4}\right)^{\frac{n}{n-1}}$$

and find when we plug this value into $c_+$

$$\begin{aligned}
&\left(\left(\frac{1}{4}\right)^{\frac{n}{n-1}}\right)^{1/2n} - 2\sqrt{\left(\frac{1}{4}\right)^{\frac{n}{n-1}}} \\
= &\left(\frac{1}{2}\right)^{\frac{1}{n-1}} - \left(\frac{1}{2}\right)^{\frac{n}{n-1}-1} \\
= &\left(\frac{1}{2}\right)^{\frac{1}{n-1}} - \left(\frac{1}{2}\right)^{\frac{1}{n-1}} \\
= &\ 0.
\end{aligned}$$

□

For any odd $n \geq 11$ we are thus given an $a$-value for which two baby $\mathcal{M}$'s of opposite critical orbits will intersect at the origin having the same center (see Figure 4.2 for an example). Now that we know these baby $\mathcal{M}$'s intersect we can actually find a whole range of $a$-values in which they will completely pass through each other as $a$ changes.

**Lemma 4.2.** *For any odd $n \geq 11$, and $\frac{1}{10} \leq a \leq \frac{(2^{n+1}-8)^2}{16}$, two baby $\mathcal{M}$'s associated with $v_-$ and $v_+$ are centered and the real axis of the c-plane and move along it as a changes.*

*Proof.* Because $a \in \mathbb{R}^+$, $c_-$ and $c_+$ lie on the real axis of the $c$-plane and Lemma 3.10 gives us that the real axis cuts the two baby $\mathcal{M}$'s in half. Since there is only one orthogonal symmetry of $\mathcal{M}$, these two baby $\mathcal{M}$'s will only move along the real axis under a changing $a \in \mathbb{R}^+$. □

Knowing that these two baby $\mathcal{M}$'s stay on the real axis as they change position, we can prove that the two sets actually pass completely through one another as $a$ changes in the given range we've been working with.

**Proposition 4.3.** *Letting $n \geq 11$ and odd, as $a$ increases from $\frac{1}{10}$ to 1, two baby $\mathcal{M}$'s associated with $v_-$ and $v_+$ move along the real axis of the c-parameter plane of $R_{n,a,c}$ in opposite directions and completely pass through each other.*

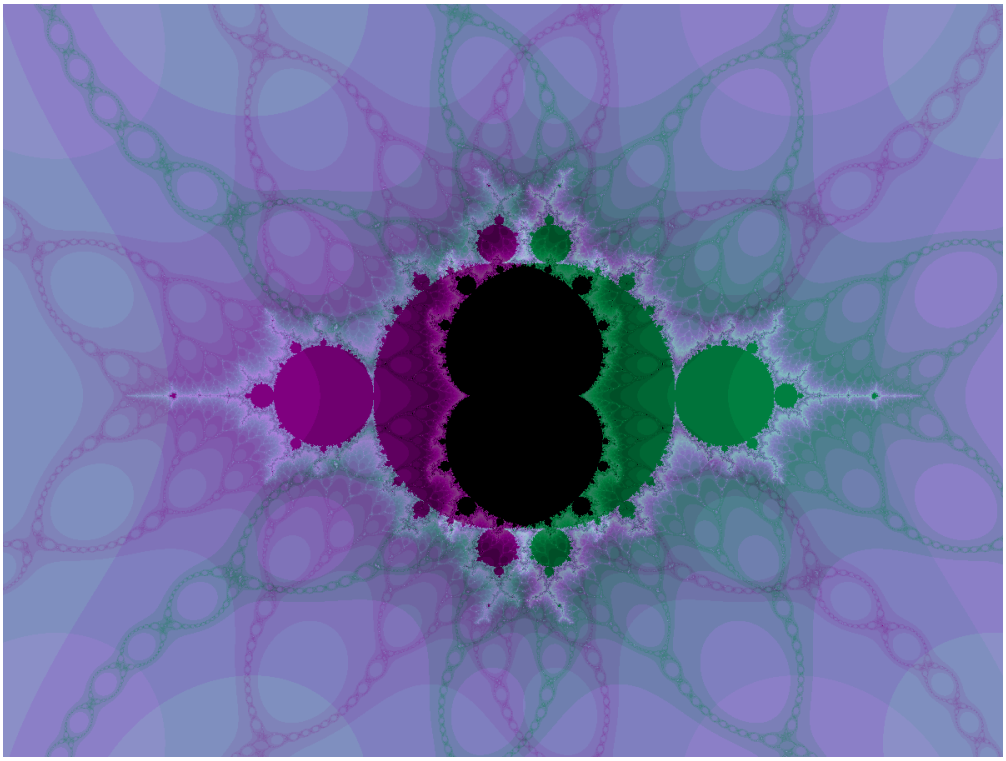

Figure 4.2: A zoom in on the $c$-parameter plane of $R_{n,a,c}$ for $n = 11$ and $a = 0.2176$ with two baby $\mathcal{M}$'s having the same exact center at the origin.

*Proof.* By Theorem 3.18 the baby $\mathcal{M}$ associated with $v_+$ lies in $\mathcal{W}_{n,a}$ with the tighter radius, this means that

$$\frac{4}{5}a^{1/n} \leq |c + 2\sqrt{a}| \leq \frac{5}{4} \;\Rightarrow\; Re(c) \in \left[\frac{4}{5}a^{1/n} - 2\sqrt{a}\ ,\ \frac{5}{4} - 2\sqrt{a}\right].$$

We refer to this interval as $\mathbf{I}_1$ and call the respective endpoints $\omega_1$ and $\omega_2$. So, any real $c$ value in this baby $\mathcal{M}$ must lie in $\mathbf{I}_1$. Because the other baby $\mathcal{M}$ associated with $v_-$ is a reflection of the first over the imaginary axis, the real values that lie in this baby $\mathcal{M}$ are just a reflection of $\mathbf{I}_1$ across the imaginary axis and so the real values of the baby $\mathcal{M}$ associated with $v_-$ lie in

$$\mathbf{I}_2 = [-\omega_2\ , -\omega_1] = \left[2\sqrt{a} - \frac{5}{4}\ ,\ 2\sqrt{a} - \frac{4}{5}a^{1/n}\right].$$

Now both of these intervals are well defined as long as $a < \left(\frac{25}{16}\right)^n$ which is true here as

$a \leq 1$. Now as we start at $a = \frac{1}{10}$ and $n = 11$, $\omega_1 > 0$ and increases with $n$ so $-\omega_1 < \omega_1$ for $a = \frac{1}{10}$ and all $n \geq 11$ and therefore $\mathbf{I}_2$ lies to the left of $\mathbf{I}_1$. As $a$ increases $\omega_1$ and $\omega_2$ decrease in value, which conversely means that $-\omega_1$ and $-\omega_2$ increase. Therefore as $a$ increases, $\mathbf{I}_1$ will move to the left as $\mathbf{I}_2$ moves to the right.

Now at $a = 1$, $\omega_2 = -\frac{3}{4}$ which is less than $-\omega_2$. Since $\omega_2$ does not depend on $n$, then for all $n \geq 11$ and $a = 1$, $\mathbf{I}_1$ lies to the left of $\mathbf{I}_2$. Therefore the two intervals have passed through each as they are both intervals of real values.

We know that they have to intersect at at least one point since Proposition 4.1 gives an $a$ value for which both baby $\mathcal{M}$'s have the same center. Lemma 4.2 shows us that the two baby $\mathcal{M}$'s had to have passed through each other since they never went away from the real axis. □

We give a few pictures of the $c$-plane in Figure 4.3 that show different phases of the baby $\mathcal{M}$'s passing through each other.

In Figure 4.4, we are given a $c$-parameter plane of $R_{n,a,c}$ satisfying the conditions of Corollary 3.20 with $a$ chosen so that we have two baby $\mathcal{M}$'s existing and overlapping. Where the two sets overlap are $c$-values for which both critical orbits are bounded. We note that one $\mathcal{M}$ in Figure 4.4 is associated with $v_+$ while the other with $v_-$.

If we zoom in closer to the green baby $\mathcal{M}$ in Figure 4.4, we can find curious black regions that occur. Figure 4.5 shows a familiar looking shape; a Julia set of $P_c$. We can see a comparison of shapes next to each other in Figure 4.6 where the two appear to be homeomorphic to each other. This is not an isolated case and other apparent Julia sets can be seen lying in these baby $\mathcal{M}$'s when they overlap. Shown in [Dev06] is the existence of an infinite number of holes in the boundedness locus of $R_{n,a,0}$ in the $a$-parameter plane. These holes are known as Sierpinski holes and are case 3 of Theorem 1.1. Sierpinski holes accumulate on the boundaries of copies of $\mathcal{M}$ at the endpoints of certain external rays discussed in Section 4.1 [Dev06]. These apparent Julia sets seem to occur on boundaries of analogous Sierpinski holes of the $c \neq 0$ case in the boundedness locus. We conjecture that

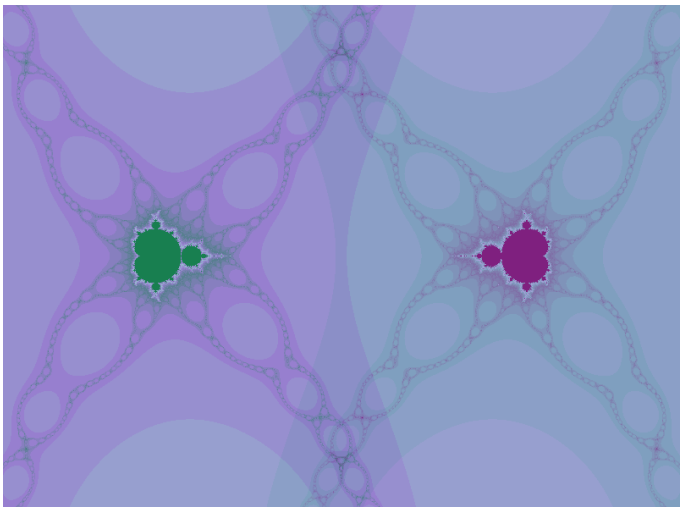

(a) Baby $\mathcal{M}$'s before intersecting

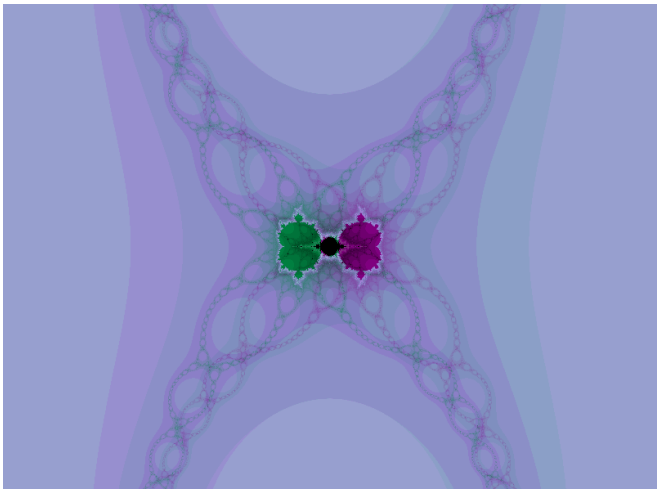

(b) Baby $\mathcal{M}$'s during intersection

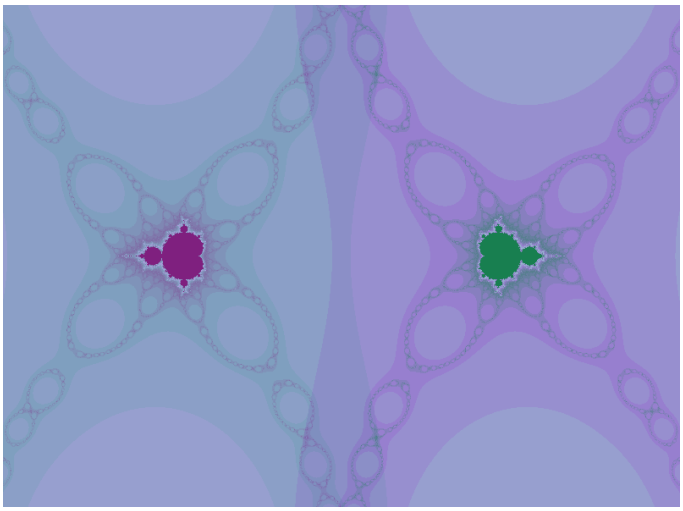

(c) Baby $\mathcal{M}$'s after intersecting

Figure 4.3: Various pictures of the $c$-parameter plane of $R_{n,a,c}$ with the phases of baby $\mathcal{M}$'s intersecting.

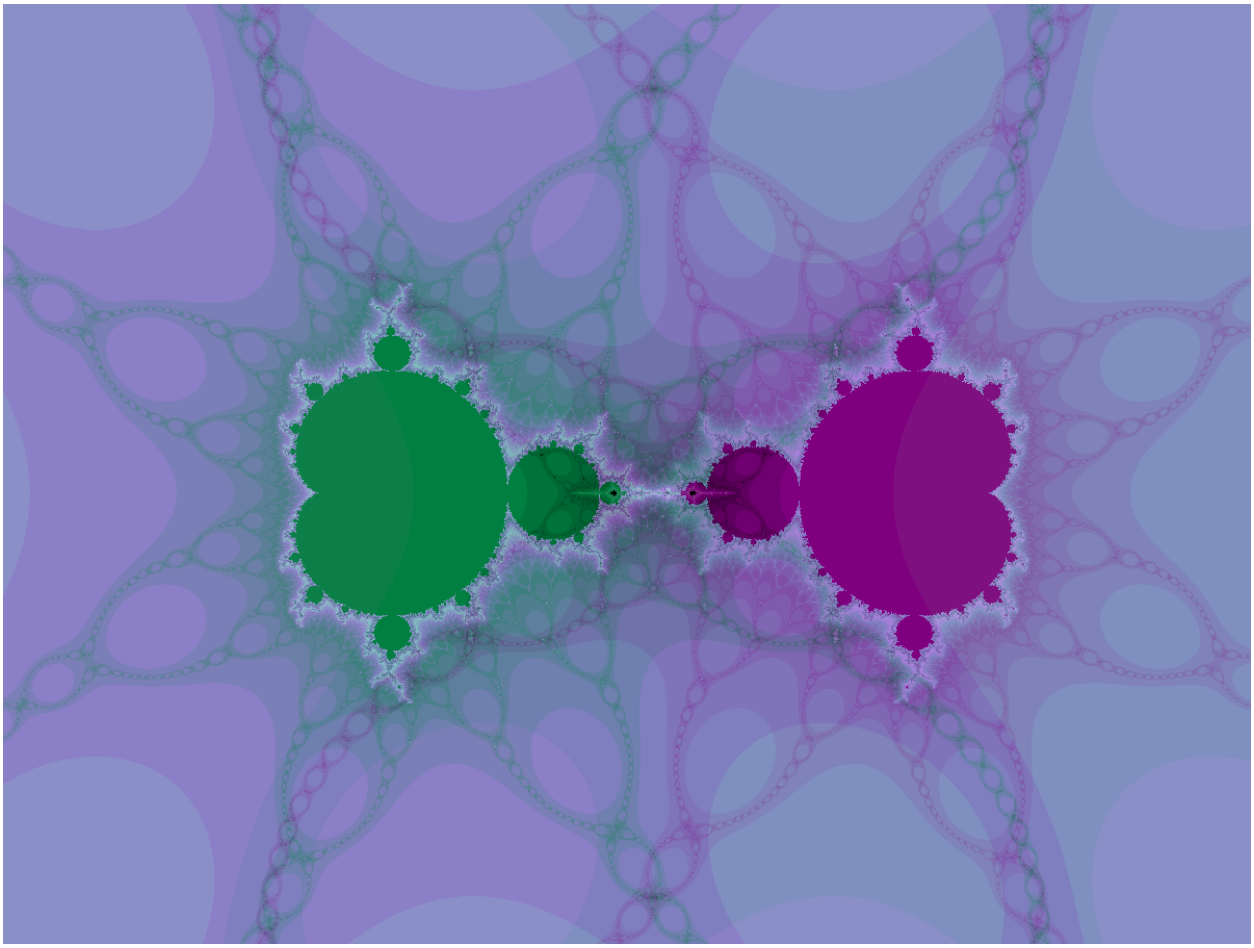

Figure 4.4: The $c$-parameter plane of $R_{n,a,c}$ with $n = 13$ and $a = 0.214$ where we see two baby $\mathcal{M}$'s overlapping.

there is a connection between these holes and external rays of baby $\mathcal{M}$'s.

These few conjectures we've made are just a glimpse of the wealth of dynamics occurring in this family. The parameter planes for $R_{n,a,c}$ are drawn based on the behavior of the individual dynamical planes. The appearance of these Julia-like objects in the parameter planes reveals new layers of complexity in the family $R_{n,a,c}$.

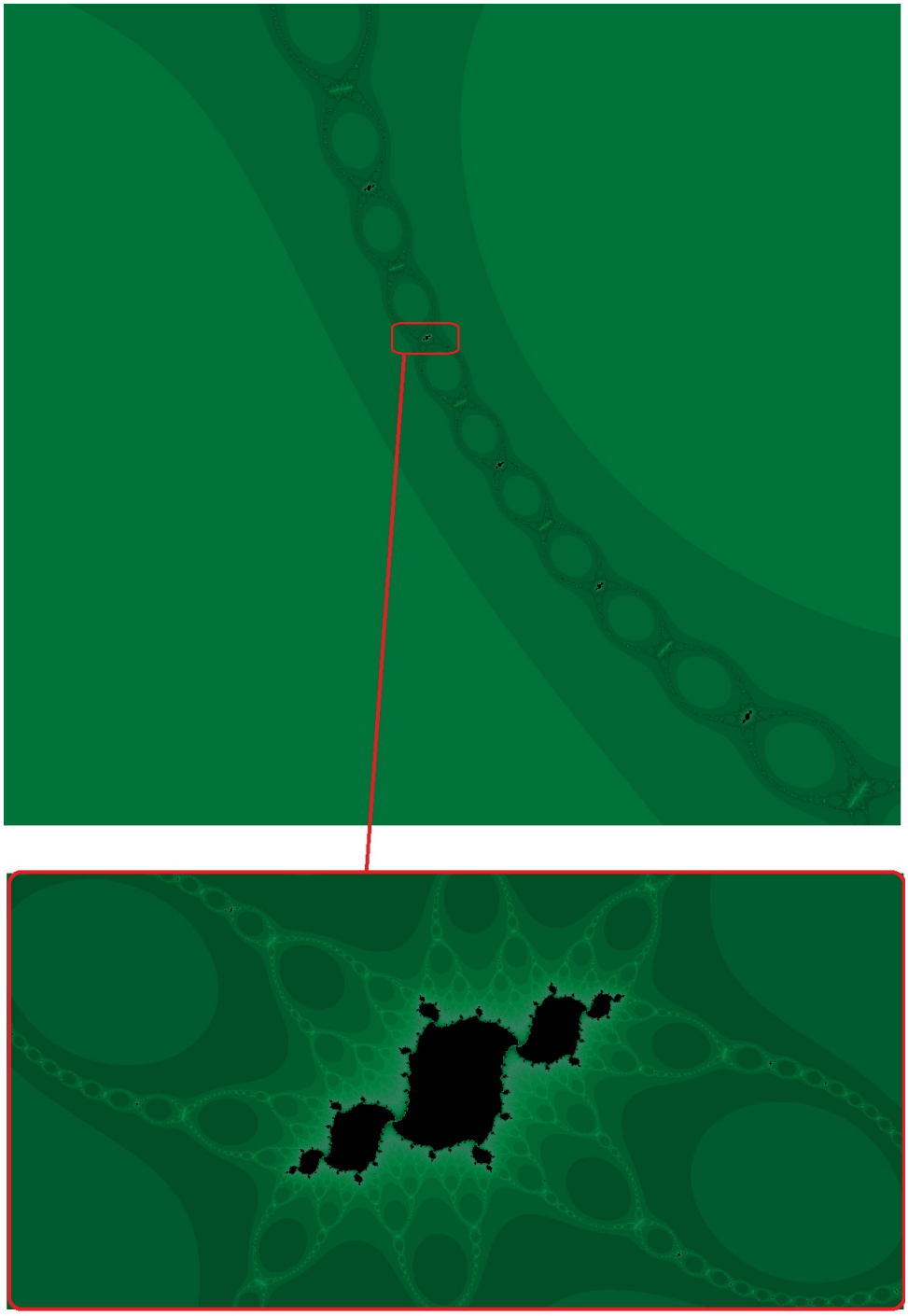

Figure 4.5: A zoomed in view of a baby $\mathcal{M}$ from Figure 4.4.

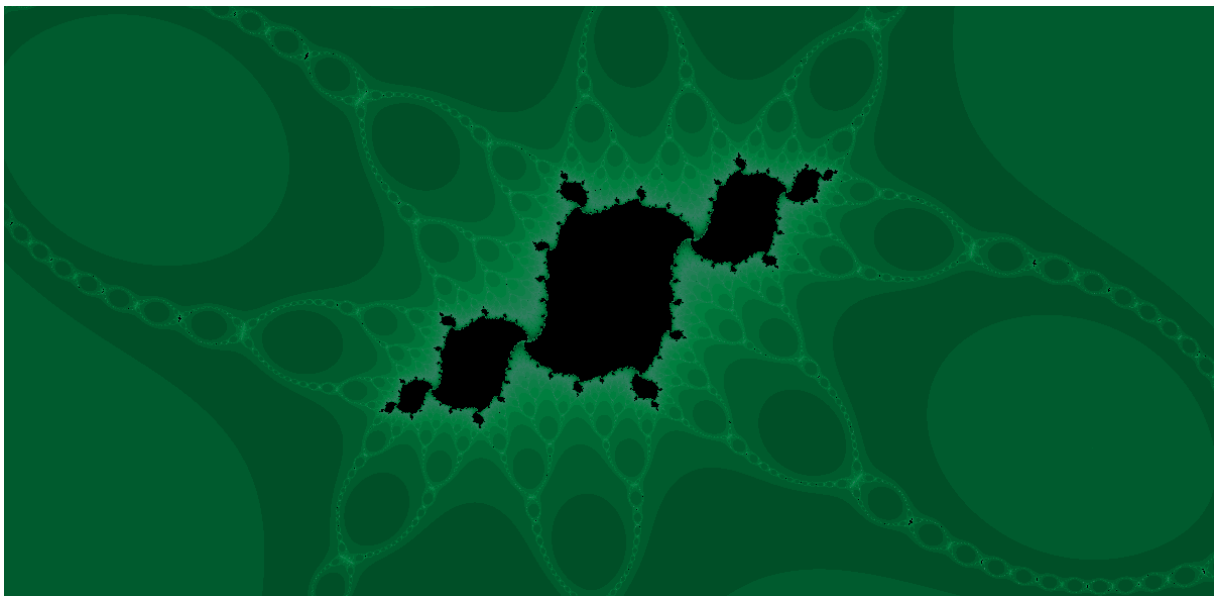

(a) An apparent quadratic Julia set in the $c$-parameter plane of $R_{n,a,c}$.

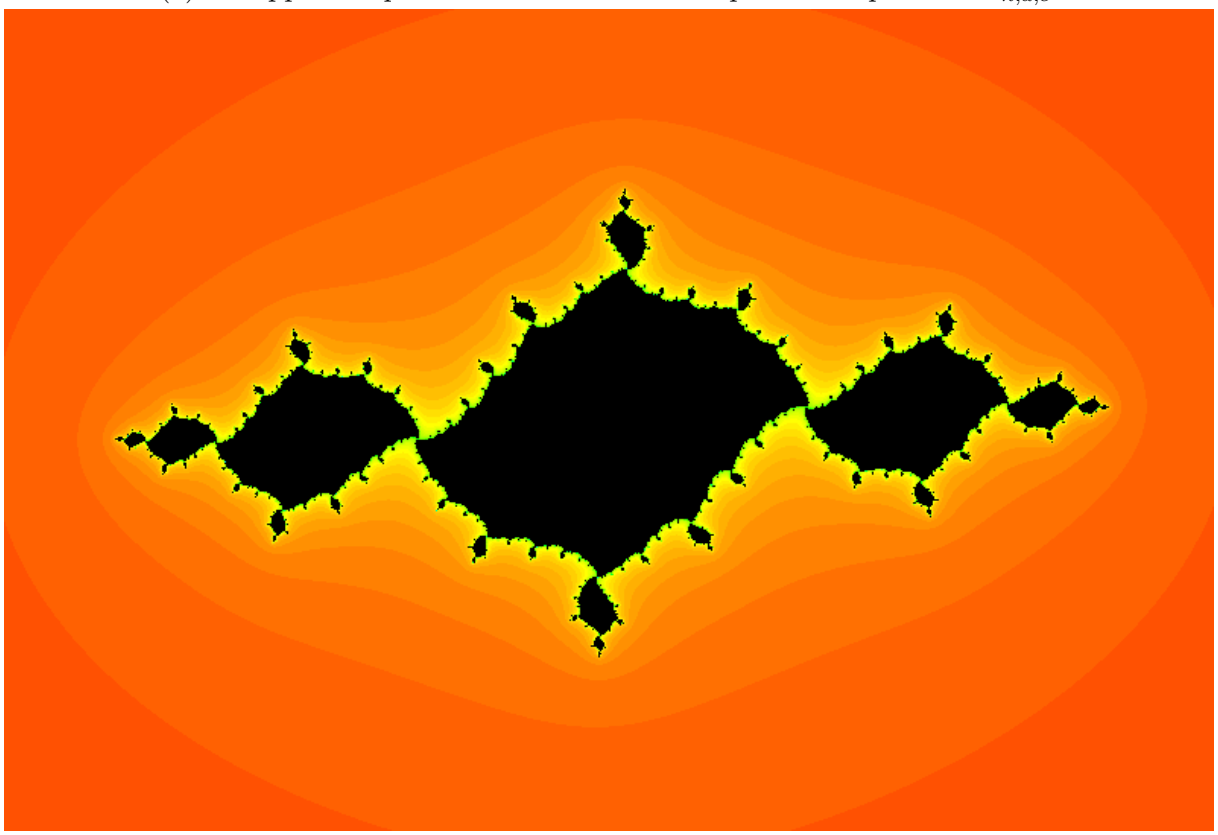

(b) Julia set of $P_c$ for $c = -1.049 - 0.1156i$.

Figure 4.6: A comparison of the $c$-parameter plane and a quadratic Julia set.

# Bibliography


[BB] Brian Boyd and Suzanne Boyd. Dynamics Explorer, at sourceforge. [http://sourceforge.net/projects/detool].

[BCDF15] Paul Blanchard, Daniel Cuzzocreo, Robert L. Devaney, and Elizabeth Fitzgibbon. Accessible mandelbrot sets in the family $z^n + \frac{\lambda}{z^n}$. 15(1):49–66, 2015.

[Bea91] Alan F. Beardon. *Iteration of rational functions*, volume 132 of *Graduate Texts in Mathematics*. Springer-Verlag, New York, 1991. Complex analytic dynamical systems.

[DBGR08] Robert Devaney, P. Blanchard, A. Garijo, and E.D. Russel. A generalized version of the mcmullen domain. *International Journal of Bifurcation and Chaos*, 18(1):2309 – 2318, 2008.

[Dev06] Robert L. Devaney. Baby Mandelbrot sets adorned with halos in families of rational maps. In *Complex dynamics*, volume 396 of *Contemp. Math.*, pages 37–50. Amer. Math. Soc., Providence, RI, 2006.

[Dev09a] Robert Devaney. Intertwined internal rays in julia sets of rational maps. *Fundamenta Mathematicae*, 206(1):139–159, 2009.

[Dev09b] Robert L. Devaney. Intertwined internal rays in julia sets of rational maps. *Fund. Math*, 206(1):139–159, 2009.

[DH85] Adrien Douady and John Hamal Hubbard. On the dynamics of polynomial-like mappings. *Ann. Sci. École Norm. Sup. (4)*, 18(2):287–343, 1985.

[GC93] Theodore W. Gamelin and Lennart Carleson. *Complex Dynamics*. Springer-Verlag, New York, 1993. Complex analytic dynamical systems.

[HS11] S. Hruska Boyd and M. J. Schulz. Geometric limits of Mandelbrot and Julia sets under degree growth. *ArXiv e-prints*, September 2011.

[McM88] C. McMullen. Automorphisms of rational maps. *Holomorphic Functions and Moduli*, 1(1), 1988.

[RLD05] David Uminsky Robert L. Devaney, Daniel M. Look. The escape trichotomy for singularly perturbed rational maps. *Indiana Univ. Math. J.*, 54:1621–1634, 2005.

[Why58] Gordon Whyburn. Topological characterization of the sierpiński curve. *Fundamenta Mathematicae*, 45(1):320–324, 1958.

## CURRICULUM VITAE

Alexander Mitchell

Place of Birth: West Allis, WI

Education

B.S., Carroll University, May 2010

Major: Mathematics

M.S., University of Wisconsin-Milwaukee, June 2012

Major: Mathematics

Dissertation Title: Existence of the Mandelbrot set in the Parameter Planes of Certain Rational Functions